Seasonally Anchored Bias Correction of CMIP5 Hydrological Simulations

M. Sierks,[a] D.W. Pierce,[a] W.E. Chapman,[b] F.M. Ralph[a]

[a] *Scripps Institution of Oceanography, UC San Diego, La Jolla, CA, USA*

[b] *National Center for Atmospheric Research, Boulder, CO, USA*

Corresponding author: M. Sierks, msierks@ucsd.edu

ABSTRACT

Robust and reliable projections of future streamflow are essential to create more resilient water resources, and such projections must first be bias corrected. Standard bias correction techniques are applied over calendar-based time windows and leverage statistical relations between observed and simulated data to adjust a given simulated datapoint. Motivated by a desire to connect the statistical process of bias correction to the underlying dynamics in hydrologic models, we introduce a novel windowing technique for projected streamflow wherein data are windowed based on hydrograph-relative time, rather than Julian day. We refer to this method as 'seasonally anchored'. Four existing bias correction methods, each using both the standard day-of-year and the novel windowing technique, are applied to daily streamflow simulations driven by 10 global climate models across a diverse subset of six watersheds in California to investigate how these methods alter the model climate change signals. Among the methods, only PresRat preserves projected annual streamflow changes, and does so for both windowing techniques. The seasonally anchored window PresRat reduces the ensemble bias by a factor of two compared to quantile mapping (Qmap), cumulative distribution function transform (CDFt), and equidistant quantile matching (EDCDFm) methods. For wet season flows, PresRat with seasonally anchored windowing best preserves the original model change over the entire distribution, particularly at the highest quantiles, and the other three methods show improved performance using the novel windowing method. Concerning temporal shifts in seasonality, PresRat and CDFt preserve the original model signals with both the novel and standard windowing methods.

SIGNIFICANCE STATEMENT

Robust and reliable projections of future streamflow are essential if we are to create more resilient water resources, and such model data must first be bias corrected. We introduce a novel windowing technique to be used in streamflow bias correction methods which improves the preservation of the original model climate change signal. Crucially, these improvements are realized not only for the water year mean signal, which is important as it relates to the total volume of water flowing through the river over the course of the year, but is also true for both low and high streamflow events which have an outsized imprint on California's hydroclimate, water resources, and ecosystems.

43

1. Introduction

a. Climate Change Impacts

Fueled by climate change, rising temperatures and declining snowpacks have revealed that the ways in which the American West has managed water for the past 75 years is insufficient to sustainably meet projected demands (Barnett & Pierce, 2009; Rajagopalan et al., 2009; Udall & Overpeck, 2017). It is equally apparent that river basins, watersheds, and reservoir drainage areas will not be impacted uniformly (Das et al., 2011; Kalra et al., 2008; Mote et al., 2005, 2018). The response of water supply-relevant variables to climate change, such as annual streamflow, total precipitation, or the extent of April 1st snowpack, will be functions of factors like shifting large-scale weather patterns, elevation, topographic aspects, vegetation, and the amplitude of season temperature cycles (Gonzalez et al., 2018; He et al., 2019; Huning & AghaKouchak, 2018; Pierce & Cayan, 2013). As a result, the potential impacts of climate change on water management, riparian health, and associated mitigation or adaptation strategies need to be examined on local scales and on a case-by-case basis.

b. Downscaling and Bias Correction

Future climate projections from global climate models (GCMs) are a key tool for estimating likely impacts of climate change on future water availability, but due to limited spatial resolution (typically no finer than 100 km) are insufficient for studying changes at the local-scale of river basins and heterogeneous hydrologic processes (Fowler et al., 2007; Hewitson et al., 2014; Salathé, 2003). Further, biases in the GCMs, arising from model limitations like subgrid parameterizations of cloud microphysics and poorly resolved topography at the native GCM grid scale, can result in distorted projected climate impacts (see discussion in Maraun et al., 2017). Prior to being used in most applications, therefore, climate projections must be downscaled and bias corrected. Implemented through either a 'statistical' or 'dynamical' approach, downscaling techniques interpolate smaller-spatial scale features by combining coarser GCM output with higher-resolution observations, topography, and dynamics to produce projections with resolutions on the order of 10s km. Either as part of the downscaling process or done subsequently, bias correction removes systematic errors in the GCM with the goal of retaining the raw GCM climate change signal.

While some climate change planning projects may be satisfied simply by downscaled and bias corrected GCM output (e.g., temperature, precipitation), many require the use of a land-surface model to produce quantities such as streamflow or soil moisture. Even if downscaled and bias corrected GCM output is used to drive the land surface model, streamflow projections often need 'secondary' bias corrections before they are used for planning due to biases introduced within the land-surface model. Though useful, it should be understood that bias correction is a statistical technique and thus is not able to discern between physical processes responsible for a given data-point or a broader climate change-imposed trend (Maraun et al., 2017).

1) WINDOWING / BIAS CORRECTION GOALS

Although the goal of the windowing and bias correction process is to remove systematic biases while retaining the signal of change from the driving climate model, many bias correction methods alter the model-predicted change for unphysical reasons (Hagemann et al., 2011; Maraun, 2013; Maurer & Pierce, 2014; Pierce et al., 2013). As a result, the application of different bias correction methods to identical datasets will yield varied future projections (Maurer & Pierce, 2014; Teutschbein & Seibert, 2012). Simplified, many bias correction methods establish a correction function that maps a model variable's empirical distribution over a historical period to that of an observed variable's distribution over a historical period. Upon applying this correction function to the model historical data, the bias corrected data is mapped onto the observed variable's distribution thus removing any systematic biases over the historical period. Though the definition of the transfer function varies among methods (Pierce et al. 2015), nearly all methods make assumptions of stationarity, i.e., that model biases occurring in the model's historical period also apply to future model periods. Though commonly adopted, stationarity is not guaranteed, and it is therefore crucial to understand under what conditions it breaks down (e.g., with changes in large-scale circulation).

Because model biases typically vary by season, correction functions are usually developed for specific calendar-based "seasons" (e.g., Thrasher et al. 2012). Specifically, distributions of the observed, historical- and future- model datasets are developed by

105 subsetting in time, either by individual months or by taking some rolling window of fixed
106 width (see Pierce et al., 2015 for a deeper discussion). Although cumulative distribution
107 functions (CDFs) can be generated either empirically (as in the methods examined here) or
108 parametrically, nonparametric methods have yielded higher skill in reducing systemic errors
109 for precipitation (Gudmundsson et al., 2012).

110 In the context of climate change, for variables whose seasonal cycles are
111 predominately affected by changing amplitudes rather than shifts in seasonality (such as
112 temperature or even precipitation) it may be fair to assume that historical biases for January
113 data can be removed directly from future January data. Consider, though, a variable whose
114 climate change signal is characterized in large part by a temporal shift in its climatology, such
115 as snowfed streamflow. Historically in the western U.S., mountainous rivers experience peak
116 streamflow during the spring (later for higher elevation sites) as the snowpack begins to melt
117 (Serreze et al., 1999). Towards the end of the 21st century, reduced in volume and melting
118 earlier, projected snowpack declines result in peak streamflow shifting significantly earlier
119 into the season (Noah Knowles & Cronkite-Ratcliff, 2018; Udall & Overpeck, 2017). If we
120 were to apply a calendar-fixed window to bias correct streamflow (e.g., comparing data from
121 the month of April, historical to future), it is possible that historical bias corrections of peak
122 or rising-limb streamflow data will be applied to future streamflow data occurring well into
123 the receding limb, thus applying corrections to and from different streamflow regimes and
124 controlled by different physical processes.

125

126 *c. Purpose of Paper*

127 Motivated by the desire to move towards a 'process-aware' method of statistical bias
128 correction and the inability of fixed calendar- windowing to account for processes that shift
129 seasonality under future climate scenarios, this paper introduces a new 'seasonally anchored'
130 windowing approach that, when applied to existing statistical methods, improves the
131 preservation of original model – used henceforth to refer to hydrologic model output driven
132 by downscaled and bias corrected GCM data – climate change signals in projections of
133 streamflow. We evaluate the performance of several published bias correction methods, using
134 the standard Julian day anchored framework and our seasonally anchored windowing
135 techniques, with respect to their ability to reduce bias while preserving key metrics of climate
136 change from the original model. Specifically, we investigate the preservation of: 1) original

model projected changes in water year mean streamflow, 2) original model projected change across all deciles of wet season streamflow, and 3) original model change in seasonality as measured by change in date of peak streamflow.

The paper is structured in the following manner. In Sections 2 and 3, we describe the study domain and the rivers included in this work, and detail the observed and model data sources used to evaluate the various bias correction methods. In Section 4, we detail the seasonally anchored windowing technique and describe the four bias correction methods compared. Section 5 describes the performance of the various methods over both the historical and future climate periods. Lastly, Section 6 summarizes and discusses these results.

2. Study Domain

The hydroclimate of California is characterized by distinct wet and dry seasons and is punctuated by high interannual variability (Dettinger et al., 2011). In fact, the presence or absence of just a few storms each year can determine the difference between drought conditions and sufficient water supply (Dettinger & Cayan, 2014). Moreover, interannual variability and dependence on just a few storms per year is expected to increase in the future, with model projections showing fewer wet days but more precipitation on the wet days that occur (Pierce et al., 2013). Because 1) there is a strong latitudinal gradient in the frequency of landfalling winter storms (Payne & Magnusdottir, 2014), and 2) interactions between low-level moisture flux and local orographic forcing is driving mechanism of California precipitation (Neiman et al., 2002), the complex terrain of coastal and inland ranges results in marked spatial heterogeneity in the hydroclimate. California's rivers and streams are as diverse as the landscapes that feed them, with flashy, ephemeral streams in low deserts and snow-fed perennial rivers in the high mountains, the latter of which are responsible for filling some of the nation's largest reservoirs. As projected climate change impacts for riparian environments differ dramatically across watersheds and stream types (Perry et al., 2015 and references therein), the diversity of California's waterways and robustness of its observational network make it an excellent testbed for our bias correction methods.

3. Data

Bias correction requires both historical (observed or reanalysis) and model data. Thus, the number of rivers eligible for examination are limited to those with both of the above datasets. Streams were selected based on the following criteria: 1) availability of routed streamflow projections from land-surface models driven by downscaled and bias corrected GCM data, 2) availability of at least 20 years of observational data, and 3) their inclusion enhance the representation of selected streams from along the continuum of rain- versus snow- dominated basins. Upon applying the above criteria, we choose 6 rivers for our case study (Figure 1, Table 1). The selected rivers span hydrologic characteristics of rain-, snow-, and mixed rain-and- snow dominated watersheds, allowing us to test the performance of our seasonally anchored windowing technique for bias correction on streams with and without large projected flow-seasonality changes. We emphasize here that our goal is not to produce an expansive dataset of bias-corrected streamflow, which requires a larger network of streams, though such an exercise will undoubtedly be useful.

Streamflow projections used in this study were obtained from Knowles & Cronkite-Ratcliff, 2018 (see Section 2.2 of Knowles and Cronkite-Ratcliff, 2018 for details). They use Localized Constructed Analogs (LOCA, Pierce et al., 2014) statistically downscaled GCM data to force the Variable Infiltration Capacity (VIC) hydrological model (Liang et al., 1994). Rather than use each of the 31 members in the Coupled Model Intercomparison Project (CMIP5; Taylor et al., 2012) ensemble, we focus our analysis on a subset of 10 GCMs chosen by the California DWR Climate Change Technical Advisory Group as providing passable simulations of the historical California hydroclimate (California Department of Water Resources Climate Change Technical Advisory Group, 2015, models listed in Table 2). Here, we restrict our analysis to the future climate relative concentration pathway (RCP) 8.5 since the climate change signal of shifting seasonality is more easily discerned in higher warming scenarios. However the results found here will apply to other emissions scenarios. Observational data for the six streams span water years (WYs) 1997-2019 and were obtained from the United States Geological Survey (USGS) and California Department of Water Resources (DWR) Data Exchange Center.

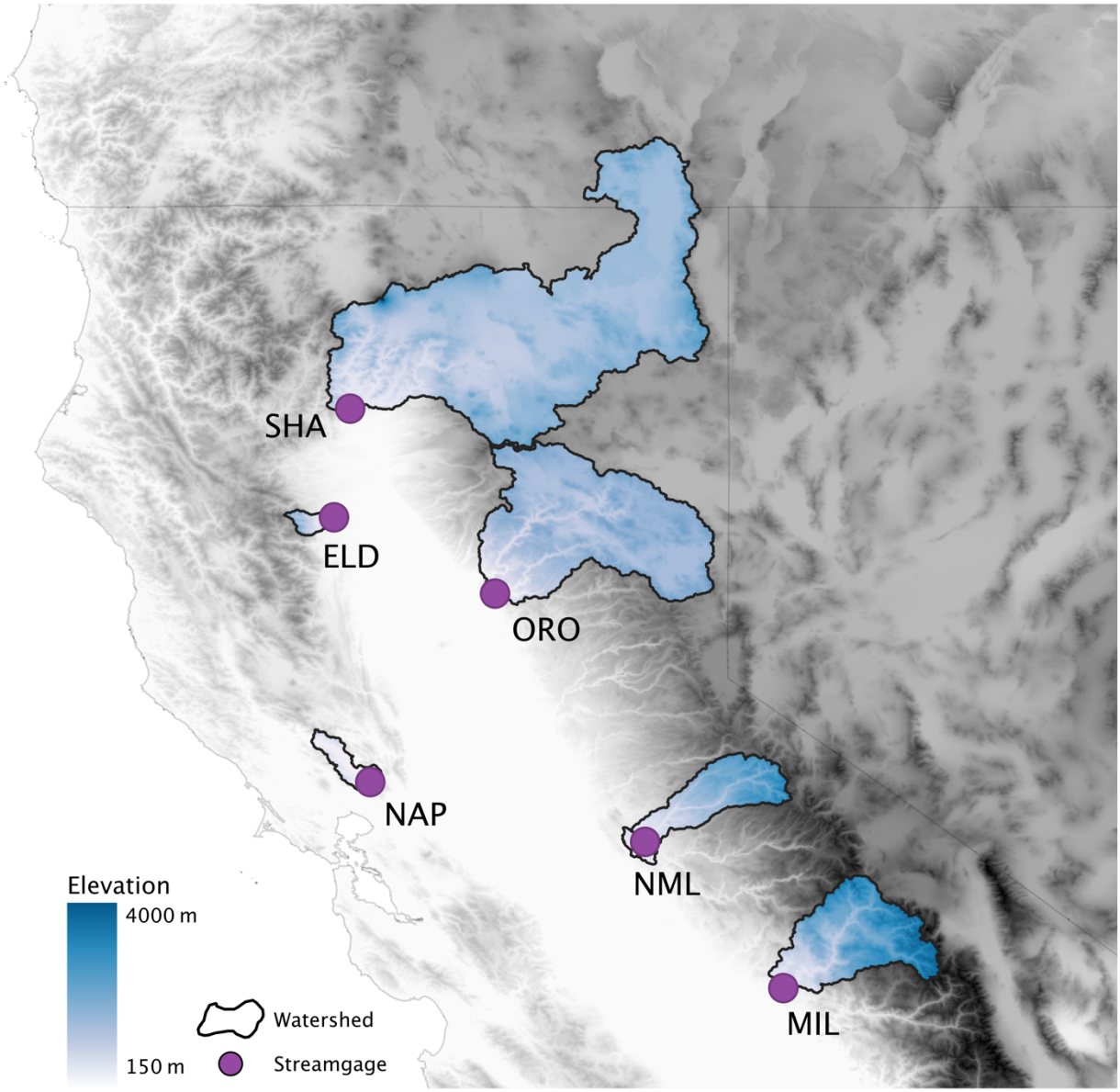

197

198 Fig. 1. Map of the study domain with watershed boundaries (black contour), gage locations
199 (purple circle), and three-letter abbreviations for the 6 streams alongside elevation (color
200 shade). Characteristics of each watershed are listed in the accompanying table.

201

Stream	Gage ID	Drainage Area (km2)	Min, Max	Mean Elevation (m)	% Streamflow

			Elevation (m)		Before April 1 (Observed)
Napa River	USGS, 1145800	550	7, 1161	247	87.7
Elder Creek	USGS, 11379500	250	255, 1959	978	73.2
Shasta Dam	CDEC, SHA	18350	306, 4113	1435	62.0
Oroville Dam	CDEC, ORO	9350	240, 2635	1545	58.0
New Melones Reservoir	CDEC, NML	2550	160, 3381	1632	43.6
Friant Dam (Millerton)	CDEC, MIL	4250	157, 3954	2161	30.6

202 Table. 1. Name, gage identification and summary characteristics of each watershed. Streams
203 are listed by their fraction of total water year streamflow occurring before April 1 (proxy
204 used to indicate importance of snowmelt) in descending order with the snowiest watersheds
205 listed in the final rows.

206

207

Model Acronym	Model Source/Institution
ACCESS1.0	Commonwealth Scientific and Industrial Research Organisation (CSIRO) and Bureau of Meteorology, Australia
CCSM4	National Center for Atmospheric Research (NCAR), United States NCAR, United States

CESM1-BGC	National Center for Atmospheric Research (NCAR), United States NCAR, United States
CMCC-CMS	Centro Euro-Mediterraneo per I Cambiamenti Climatici
CNRM-CM5	Centre National de Recherches Météorologiques, France
CanESM2	Canadian Centre for Climate Modelling and Analysis, Canada
GFDL-CM3	Geophysical Fluid Dynamics Laboratory (GFDL), Princeton, New Jersey, United States
HadGEM2-CC	Met Office Hadley Center, UK
HadGEM2-ES	Met Office Hadley Center, UK
MIROC5	Atmosphere and Ocean Research Institute and NIES, Japan

Table. 2. Selection of 10 GCMs from CMIP5 used in this work along with their originating institutions.

4. Methodology

While the following subsections describe the methodology in complete detail, we preface by briefly summarizing the algorithmic approach. First, for a given value that is to be bias corrected, we convert from Julian day to a hydrograph-relative time unit. This is done by locating its position (in time) relative to important climatological features (e.g., day of peak streamflow). Then, we map this point in 'hydrograph-relative' time onto all datasets (observed, historical GCM, future GCM) to identify hydrologically similar periods.

a. Climatological Hydrograph

The first step in the new seasonally-anchored approach is to calculate climatological mean hydrographs for the (1) observed, (2) simulated-historical and (3) simulated-future flows. In the present study, the length of climatological periods varies from the observed

(n=23 years, 1997-2019), simulated-historical (n=36 years, 1970-2005), and simulated-future flow series (n=31 years, e.g., 2069-2099). The observed period is limited by the period of available record of gaged streamflow. Climatological-average hydrographs are computed at several quantiles (discussed below), but to ease explanation of the process, we explain it for the 70th percentile (P70) first.

For a given Julian day, the 70th percentile streamflow value is estimated from a distribution containing all data from the climatological period within a 31-day centered window (e.g. at Julian day 185, use data from Julian days 170-200) similar to Thrasher et al., 2012. Once done for all days of the year, this array of length 365 is then smoothed by taking the mean of all points within the centered 31-day windows. The resulting smoothed array is the climatological hydrograph at the 70th percentile (Figure 2, top).

b. Locating Seasonal Milestones

Once the climatological hydrograph is calculated for a given percentile, milestones along the curve that correspond to key characteristic features of the stream are identified. Similar to previous work by Yarnell et al. (2015) we define our milestones as the Julian days when four climatological-hydrograph transitions occur (detailed below, and shown in Fig. 2): (1) minimum flow, (2) transition from a low-flow period to the rising limb, (3) maximum flow, and (4) transition from the receding limb to a low-flow period.

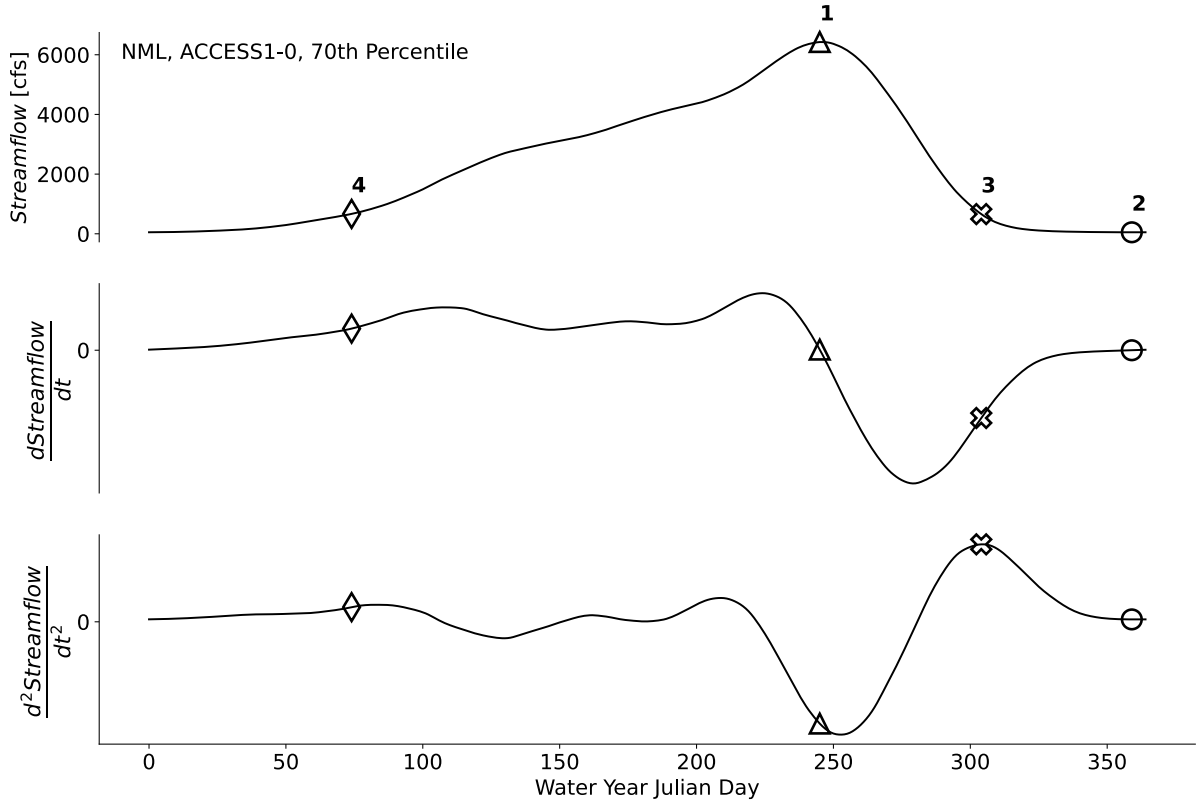

242

243 Fig. 2. Visual depiction of the algorithm used to identify climatological milestones for the
244 seasonally anchored windowing method. Climatological data from the New Melones stream
245 and ACCESS1.0 GCM is shown at the 70th percentile to illustrate the method. Daily mean
246 climatological streamflow (top), and the first and second derivatives of streamflow with
247 respect to time (middle and bottom respectively) are plotted on against water year Julian day.
248 Numerical annotation is used to indicate the workflow by which the four seasonal milestones
249 are assigned: (1) Peak streamflow (triangle), (2) Minimum streamflow (circle), (3) Start of
250 the dry season/end of receding limb (x), and (4) Start of the wet season/beginning of the
251 rising limb (diamond).

252

253 1) MAXIMUM AND MINIMUM STREAMFLOW

254 The milestone of peak flow occurs on the Julian day with the largest climatological
255 streamflow and delineates the change from the rising to the falling limbs of the hydrograph
256 (Fig. 2, triangle). Similarly, the milestone marking the minimum streamflow occurs on the
257 Julian day with the lowest value of climatological streamflow (Fig. 2, circle). This is done for
258 each of the three flow series. Although the vast majority of climatological hydrographs in this

study are described by having a single peak, Appendix A describes how the identification of the peak streamflow milestone is handled for 'bimodal' hydrographs.

2) START OF DRY SEASON

Qualitatively, transitions between distinct streamflow regimes occur when the shape of the hydrograph changes rapidly. We can quantify the shape of the hydrograph by its 1st and 2nd derivatives with respect to time. The first derivative of streamflow ($\frac{dQ}{dt}$, Figure 2 middle) indicates where the stream is rising and falling. If we wish to pinpoint the end of the falling limb, we must only examine days when $\frac{dQ}{dt} < 0$. The second derivative with respect to time ($\frac{d^2Q}{dt^2}$, Figure 2 bottom) is used to identify when the hydrograph has maximum points of curvature, or in the language used above, when the shape of the hydrograph indicates an inflection point. To identify the milestone associated with the end of the falling limb (start of the dry season), we find the Julian day coinciding with the local maximum of $\frac{d^2Q}{dt^2}$ given that $\frac{dQ}{dt} < 0$. This is shown schematically in bottom subplot of Figure 2 by the 'x'. This is done for the observed and simulated-historical datasets. The process for the simulated-future dataset is describes in the following section.

3) START OF WET SEASON

For mixed rain- and snow dominated rivers, there is larger variability in the onset of the wet For mixed rain- and snow dominated rivers, there is larger variability in the onset of the wet season than the onset of the dry season (Patterson et al., 2020) as the former is governed by precipitation, which has a high degree of interannual variability (Dettinger et al., 2011), whereas the latter is corresponds to the end of the snowmelt pulse (Stewart et al., 2005), which is driven by lower variability fields such as synoptic temperature advection and solar insolation (Cayan et al., 2001; Mioduszewski et al., 2015; Pederson et al., 2011). Therefore, we don't apply the same method as in the previous section. Rather, we assume the streamflow value associated with the 'start of the dry season' milestone delineates between baseflow and non-baseflow periods. Since the 'start of the wet season' marks the stream's departure from baseflow, the corresponding milestone is set at the Julian day when the

climatological hydrograph increases above the streamflow value associated with the 'start of the dry season' milestone. This is shown schematically in top panel of Figure 2 by the diamond marker and is calculated for the observed and simulated-historical datasets.

Motivated by the importance of the low-flow period to ecosystem health (Hill et al., 1991; Petts, 1996; Poff et al., 1997; Richter et al., 1996), we deem this 'threshold value' (evaluated as flow above baseflow) to be characteristic of the stream and assume that the streamflow above baseflow value associated with the low-flow period does not change with time. That is, while baseflow levels may change from historical to future periods, if the historical low-flow period was delineated at 500 cfs above baseflow, then the future climate milestone for the 'start ('end') of the west season' will be located when the stream rises (falls) to 500 cfs above the future climate baseflow. This will yield a consistent comparison of how both the duration of the low-flow period and corresponding streamflow magnitudes change in future climate projections.

c. Calculating the Mean Milestones Across Quantiles

The milestone identification process is performed with hydrographs computed at every 5 percentage points between the 40^{th} and 80^{th} percentiles (P40-80). The final milestone locations for the climatological period are computed by taking the mean value of the milestone dates across all individual quantiles. The rationale for choosing to evaluate data between the 40^{th} and 80^{th} percentiles is two-fold. First, the final milestones should represent a broad range of climatological stream conditions, but extreme values—while only a small fraction of total data--can yield outlier milestones that are not representative of the entire distribution. Because of this, quantiles near the distribution tails are excluded from this final step of the milestone process – though they are accounted for during the windowing procedure described in Section 4.d. Second, the asymmetry, relative to the median, of the P40-80 range reflects the differing dynamics of high and low flow climatologies. High quantile flows in the early water year only occur when the synoptic environment is favorable for large precipitation events (typically October at the earliest). As a result, for higher quantile climatological hydrographs, the timing of the start of the wet season is more-or-less constrained to a narrow window of 1-3 months at the beginning of the water year. However, low quantile flows correspond to the absence of large storms and are not constrained in time. For drier years with few storms during the early WY, the start of the wet season can be

pushed far into the water year and, if included, skew the mean value taken over all quantiles in P40-80 (see Fig. A2 and A3).

d. Seasonally Anchored Windowing

Using the milestones as reference points, we are able to bias correct a day's simulated flow in a way that acknowledges its position in the hydrograph, which ensures that the hydrologic processes at work on that day are accommodated. For example, a flow that occurs on the descending limb of the hydrograph will be bias corrected using the same parameters no matter whether that flow is in, e.g., June in the historical period or in, e.g., April in a future projection (Fig. 3, bottom). This differs from traditional bias correction techniques that are anchored by day-of-year, which means (in cases where the peak flow shifts earlier in the year) the bias correction parameters from the rising limb of the hydrograph in the historical period might be applied to values from the descending limb of the hydrograph in the future period (Fig. 3, top). Because window widths are based on the length of streamflow regime segments (e.g., rising limb), and those segments vary across the observed, historical-, and future GCM climatologies, we do not require the different datasets to have the same window widths. Before the actual bias correction step is done, the empirical distributions of daily streamflow data are cubic hermite spline interpolated to obtain the same length, following Pierce et al., 2015.

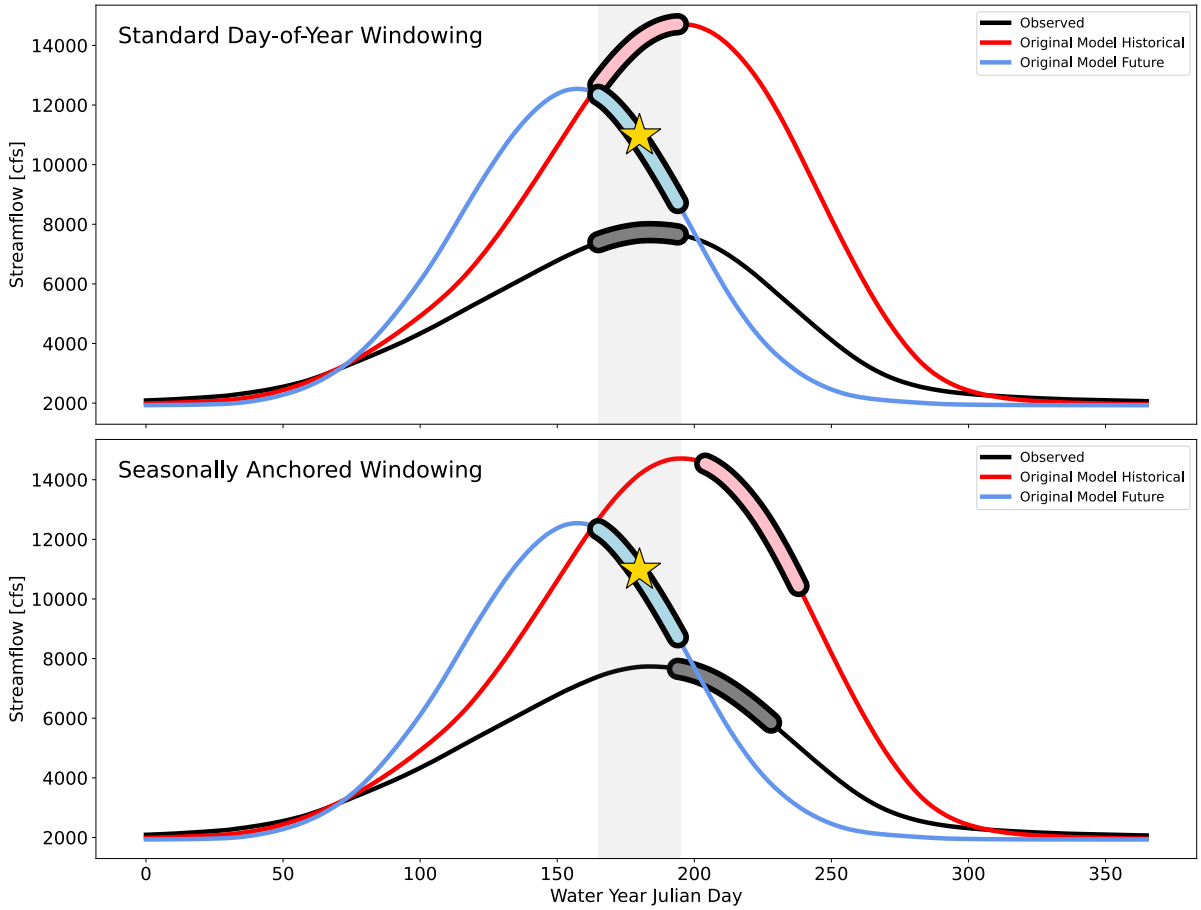

Fig. 3. Schematic highlighting the effect of windowing technique on which segments of the climatological hydrograph are used to bias correct a given model datapoint on the 180th day of the water year (yellow star). Each panel shows the climatological hydrographs in thin lines for the observed (black), historical original model (red), and end-of-century original model (blue) data. The segments of each hydrograph used in bias correction are plotted as bolded lines. Standard day-of-year windowing (top) uses data from each curve that falls within the centered 30-day period (grey shaded region). Seasonally anchored windowing (bottom) uses a centered 30-day window over the climatological period being corrected and then finds equivalent segments of the observed and historical hydrographs to use for bias correction.

e. Bias Correction Methods to be Compared

To illustrate the effect of the windowing technique on bias corrected streamflow data, we examine the performance of 4 different bias correction methods using first the standard DOY windowing, and then seasonally anchored windowing. Similar to (Pierce et al., 2015), we apply the following techniques: PresRat (Pierce et al., 2015), CDF-transform (CDFt,

Michelangeli et al., 2009), equidistant CDF matching (EDCDFm, Li et al., 2010), and quantile mapping (Qmap, Panofsky & Brier, 1968; Wood et al., 2002). For the sake of brevity, we do not discuss the details of each bias correction method and instead refer the reader to Section 3 of Pierce et al., 2015.

For the CDFt, EDCDFm, and Qmap methods, we adopt the standard practice of bias correcting data using a 30-day window centered around a given datapoint. The 30-day window enables the methods to represent the seasonal cycle, but such a narrow window is not suitable to correct extreme events. Because extreme values of precipitation can occur at any time during the wet season, the PresRat method from Pierce et al., 2015 does not use a fixed 30-day window like the other 3 methods and instead iteratively bias corrects data using windows of increasing width, providing better correction of extreme values. Rather than applying iterative bias correction in the version of PresRat used in this study, we develop an alternative method to balance the correction of extreme values (requiring a wide window) and the seasonal cycle (requiring a narrow window). Here, we vary the window width based on the 'extremity' of a value. Beginning with a 30-day window, we find the quantile location of the data point being corrected in its climatological distribution. If it falls between the 20^{th} and 80^{th} percentile, a 30-day window is used. Otherwise the window is expanded by 15-days on either side and the quantile location of the data is found again. If the data falls between the 10^{th} and 90^{th} percentile, the 60-day window is applied. If not, a 120-day window is used to bias correct the most extreme values. This reflects the fact that extreme events are by nature rare.

Because some methods of bias correction operate on fractional changes between a future and historical model period, they can be sensitive to small errors occurring at low values (Pierce et al., 2015). For this reason, prior to bias correction, we correct for any biases in the model baseflow by adding the difference between the observed and simulated baseflow values to all model data. This greatly improves the efficacy of the bias correction methods at lower flows while having very little impact at higher flows.

5. Results and Discussion

The efficacy of a bias correction method can be evaluated by its ability to remove systematic model biases while preserving desired climate change signals from the original

model. In this case we choose to consider: 1) mean changes in streamflow magnitude over the entire water year, 2) changes in magnitude evaluated at high, medium, and low quantiles of the distribution, and 3) temporal shifts of seasonality (which may be small in some streams). The combination of bias correction method (QM, CDFt, EDCDFm, PresRat) and windowing technique (standard day-of-year or seasonally anchored) is evaluated by its ability to preserve the 3 quantities listed above. As the magnitude of streamflow varies substantially between California watersheds, working with normalized data allows for a more straightforward comparison of climate change signals. For this reason, we normalize any change between a simulation's future and historical values by a historical baseline (Equation 1) to give a percent change relative to the pre-climate change period.

$$\Delta = \mathbf{100} * \frac{\boldsymbol{Future - Historical}}{\boldsymbol{Historical}} \quad (1)$$

Using a standardized metric (Δ) helps us compare both the magnitude of change across a diverse subset of streams and the performance of bias correction methods in preserving this metric. In the following sections, we evaluate change between the future (also referred to as 'end-of-century') and historical periods defined as water years 2069-2099 and 1970-2005 respectively. Subsequent sections evaluate this change over both the entire water year and over the 'wet season', which we define as the timeframe spanning 1-month prior to the start of the wet milestone to 1-month after the end of the wet season milestone. This covers the period roughly from November to June (although it is subject to both watershed elevation and climatological era).

a. Validation over the Historical Period

Applied over the historical period, the PresRat, CDFt, and EDCDFm methods simplify to the quantile mapping method, with the exception of data off the endpoints of the historical distribution (see Section 3 of Pierce et al., 2015 for discussion). Therefore, when using a relatively narrow 30-day window, all methods are effective in correcting the historical GCM data so that it recreates the observed data's seasonal cycle. This is true for both the standard day-of-year windowing technique and the seasonally anchored windowing technique (not shown). Concerning the historical period, the only meaningful difference between the four bias correction methods results from the variable window width used in our PresRat

method (Figure 4). Because the window width expands when correcting high-quantile data, large streamflow events occurring early in the wet season can be mapped onto observed streamflow values occurring up to 60 days later (as opposed to 15 days later in the standard method). This can result in slightly elevated mean flows during the transition from dry-to-wet season, driven by streamflow at high quantiles. However, as extreme precipitation and streamflow events can occur at any point between October-April, a variable window based on the quantile of the datum being corrected is more easily justifiable than the common fixed narrow (31-day) window when correcting hydrometeorological variables in the western US.

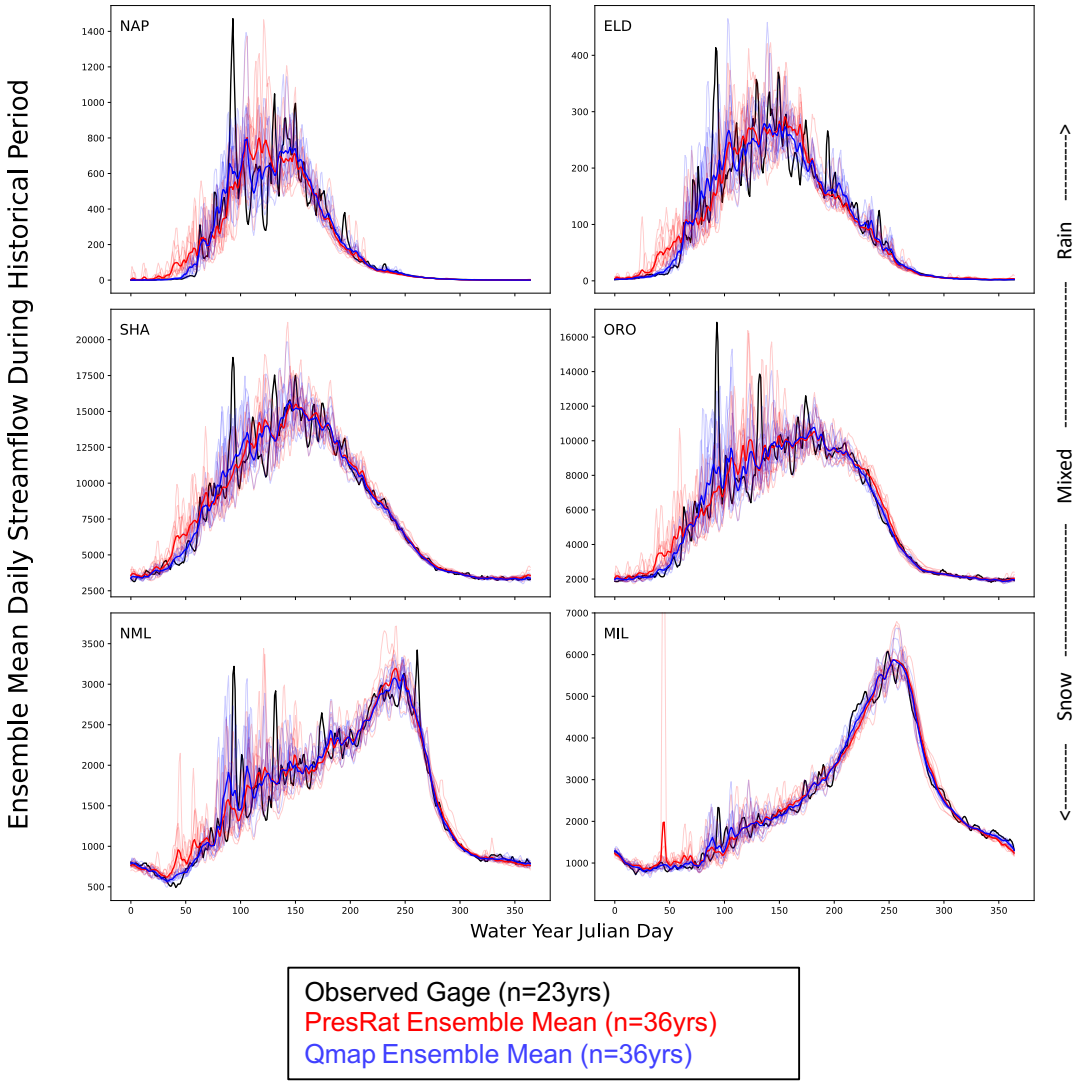

Fig. 4. Daily mean streamflow for the observed (black), and bias corrected data over the historical period for PresRat with seasonally anchored windowing (red) and quantile mapping with day-of-year windowing (blue) for each of the 6 rivers. For the GCM data, the ensemble mean across the 10-GCMs is shown in a bolded line with individual members depicted by

thin lines. Subplots are arranged such that from top-to-bottom, streams transition from rain- to snow dominated watersheds.

b. Water Year Mean Streamflow

Before evaluating the ability of each bias correction method to preserve the projected future change in mean water year streamflow, we first examine the original model signal (Figure 5). Across the simulations of 6 streams that were driven by projections from 10 GCMs, the changes in water year mean streamflow differ considerably. Evaluating change in units of percent of historical mean, which removes the influence of differing streamflow magnitudes, we see that CESM1-BGC, CNRM-CM5, and CanESM2 have the largest projected increases in water year mean streamflow with values upwards of 40% for some streams. Although the largest percent increases occur for the streams with the lowest flows, these models suggest higher-flow streams will still see increases beyond 30%. Among the projections based on the 10 GCMs, there is little agreement on the sign or magnitude of the projected change and the projections with very large increases heavily influence the multi-model ensemble mean change.

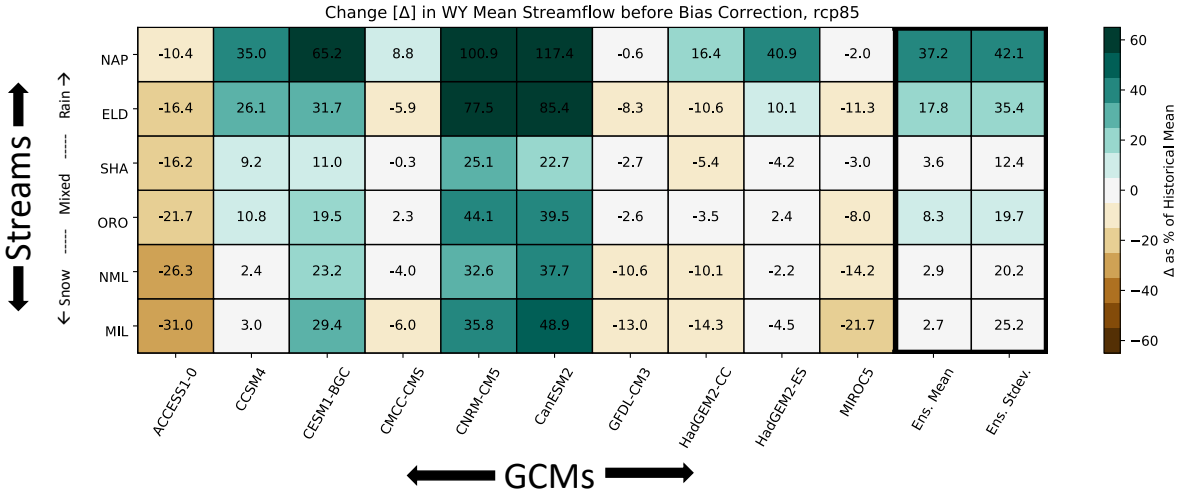

Fig. 5. Original model projected change in water year mean streamflow across the 6 streams (rows) and 10 GCMs (columns) with the 10-member ensemble mean and standard deviation (farthest right columns). Using units of 'percent change from the historical mean', increasing streamflow is indicated by green color-shading, and decreasing streamflow by brown. Values under 5% change appear as white.

453

454 We use the term 'error' here to refer to the difference between original model
455 projected change and post-bias correction projected change. This quantity is an error in the
456 sense that we expect our bias correction approach to preserve certain key aspects of the
457 model-predicted climate change signal (as listed explicitly above), and is defined in Equation
458 2 below,

459 $$Error = \Delta_{Bias\ Corrected} - \Delta_{Raw\ GCM} \quad (2)$$

460 wherein Δ is defined by Equation 1. Using the above definition, we now compare the ability
461 of the 4 bias correction methods and 2 windowing techniques in preserving the signal of
462 water year mean change averaged across the 10 GCMs and 6 streams.

463 The CDFt, EDCDFm, and Qmap bias correction techniques do not intrinsically
464 preserve the water year mean flow change signal from the un-bias corrected projections
465 (Table 3). The PresRat method is the one method that preserves the water year mean flow
466 change, for both windowing methods, with mean and root-mean-square (RMS) errors <1%,
467 and does so by design (see Pierce et al., 2015). The other three methods alter the original
468 model signal to varying degrees. In all cases, applying a seasonally anchored window
469 improves the preservation of the water year mean flow change signal by nearly a factor of 2
470 compared to the standard day-of-year windowing technique. In addition to improving the
471 mean flow change, the new windowing technique also results in a narrower spread of errors
472 among the models in the PresRat, CDFt, and Qmap methods.

473

BC Method	Ens. Mean Error [%]	RMS Error [%]
PresRat	0.20 (0.37)	0.86 (0.91)
CDFt	1.72 (6.18)	5.57 (8.64)
EDCDFm	4.49 (7.69)	13.04 (12.96)
Qmap	3.33 (6.14)	7.64 (10.59)

474 Table 3. Summary statistics for each bias correction method (rows) and windowing technique
475 (Standard day-of-year show in parentheses, seasonally anchored shown without) on their

476 success in preserving the projected mean change in water year mean streamflow across the 6
477 streams and 10 GCMs.

478

479 *c. Wet Season Streamflow by Decile*

480 The hydroclimate of the western US is dominated by the occurrence (and absence of)
481 extreme precipitation and streamflow events. Therefore, statistical bias correction techniques
482 need to preserve the original-model projected changes at high-flow quantiles, rather than
483 altering the projected change for no physical reason. When viewed at the granularity of a
484 single percentile of flow, the signal of projected changes can be noisy. Therefore, we evaluate
485 here changes at decile levels over the wet season. Again, before evaluating the ability of each
486 bias correction method to preserve this quantity, we first examine the un-bias corrected model
487 signals. Change is calculated with Equation 1 using the mean of all streamflow values within
488 a given decile range for each of the historical and future climate periods. Figure 6 gives a
489 visual depiction of the original model climate change signal at the Shasta gage and the
490 remaining 5 streams can be seen in Appendix B. Although some minor differences exist
491 among the 6 streams and 10 GCM-based histories, there is a near unanimous agreement that
492 the top 10-20% of streamflow values will increase while the middle ~30% of the distribution
493 will decrease. This follows the projected climate change signal in precipitation wherein high-
494 tail events occur with greater frequency (Gershunov et al., 2019). Notably, in the historically
495 most snow dominated watershed, Millerton, larger differences exist between the 10-member
496 ensemble, with 4 models projecting large increases at the high end and 2 projecting
497 decreases. Again, this work does not focus on the impacts or certainty of projected
498 streamflow changes, but rather on the extent to which they are altered by bias correction
499 techniques.

500

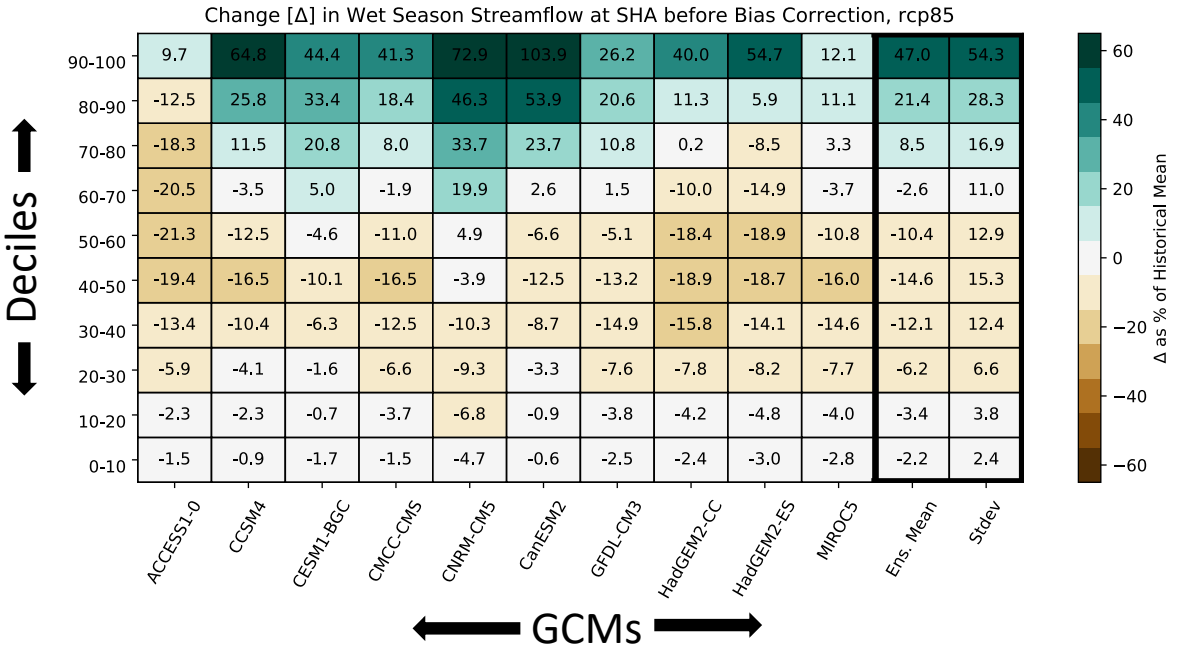

Fig 6. Original model projected change in Shasta streamflow by decile (rows) and GCM (columns) with the 10-member ensemble mean and standard deviation (farthest right columns). Using units of 'percent change from the historical mean', increasing streamflow is indicated by green color-shading, and decreasing streamflow by brown. Values under 5% change appear as white.

Using Equation 2, we evaluate how well each correction method and windowing technique preserves the original projected change at each decile over the wet season. Figure 7 provides a visual representation of these errors for the PresRat method using seasonally anchored windowing. Equivalent plots for the remaining combination of bias correction and windowing methods can be found in Appendix C. Each subplot contains a box-and-whisker plot for a given stream wherein errors for individual GCM projections are shown by grey circles and the mean error across the 10-member ensemble is depicted by an orange line. In Figure 7, with few exceptions, errors in the depiction of future changes in wet season streamflow, by quantile, falls within ± 10% of the original model signal for all the combinations of GCMs and streams. As mentioned earlier, a large fraction of the total streamflow is contained in the top 10-20% of the distribution. To highlight where, in terms of decile, large errors in the bias correction method begets large errors in streamflow, the fraction of total wet season streamflow represented by each decile is plotted on the right y-

axis. Though not explicitly shown here, the PresRat method with seasonally anchored windowing has notably smaller biases than other techniques at the top decile of flows.

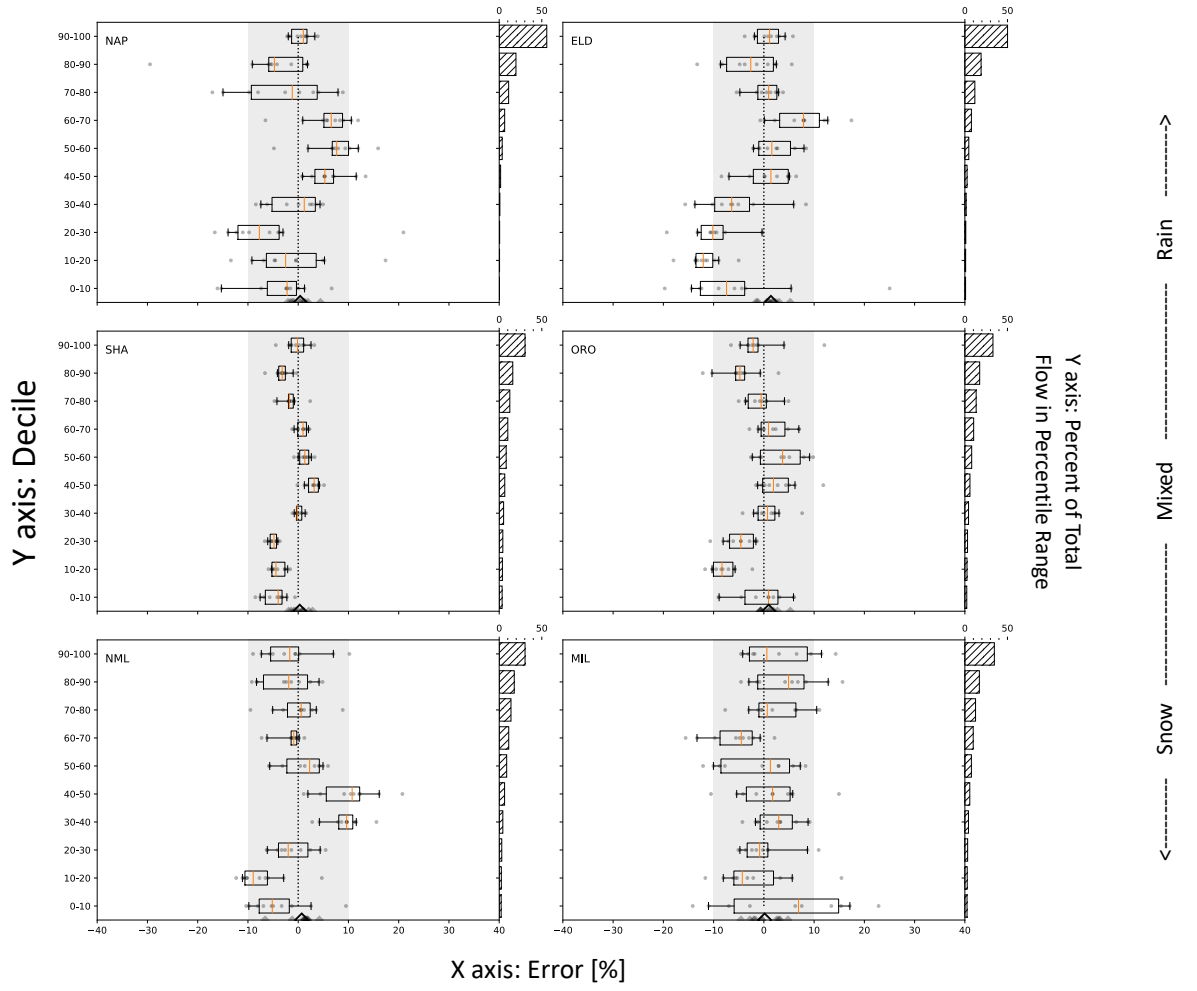

Fig. 7. Error by decile for change in wet season streamflow for PresRat with seasonally anchored windowing. Errors (x-axis) for individual GCMs are depicted by grey circles, the mean error across the 10-member ensemble is depicted by an orange line. The box edges and whiskers represent the middle 5 and 8 GCMs respectively. The error for a single GCM averaged over all deciles is depicted as a small grey triangle on the x-axis and the value for the 10-member ensemble mean is denoted by a large triangle. For reference, the grey shading and dashed black line correspond to ± 10% error and 0% error respectively. For each stream, the right y-axis depicts the historical percentage of total wet season streamflow contained in each decile averaged across the 10-member ensemble. Subplots are organized so that as you move down the rows, streams transition from rain- to snow dominated over the historical period.

To quantitatively assess how well the original signal is preserved, we calculate the root-mean-square error (RMSE) at each decile for each of the 4 correction methods and 2 windowing techniques, using the following equation,

$$RMSE = \sqrt{\frac{\sum_{i=1}^{N}(\Delta_{Bias\ Corrected_i} - \Delta_{Raw\ GCM_i})^2}{N}} \quad (3)$$

where i represents a given driving-GCM. Then, motivated by the importance of large streamflow events to the hydroclimate of the western US, we weight the RMSE at each decile by the percentage of total historical wet season streamflow in the decile, thus emphasizing errors at higher deciles. We refer to this quantity as the flow-weighted RMSE. To equally weight the performance of the bias correction technique on each river, and thus equally sampling the range of snow vs. rain dominated regimes, the flow weighted RMSE at each decile is averaged across the 6 streams.

Figure 8 and Table 4 summarize the above process and depicts the flow weighted RMSE averaged across the 6 streams for all combinations of correction method and windowing technique. At lower deciles, the flow weighted RMSE values are similar across the 4 correction methods. The lines begin to diverge near the 50th percentile with the seasonally anchored PresRat and CDFt methods achieving the best performance between the 50th-90th percentiles. For the top 10% of streamflow, where the most impactful of streamflow events exist, PresRat with seasonally anchored windowing best preserves the original model signal of change. If we take the average across all deciles for each line individually, we see that the PresRat method using seasonally anchored windowing not only yields the lowest flow weighted RMSE, but that for each correction method, the seasonally anchored windowing method outperforms the standard day-of-year method (triangle markers).

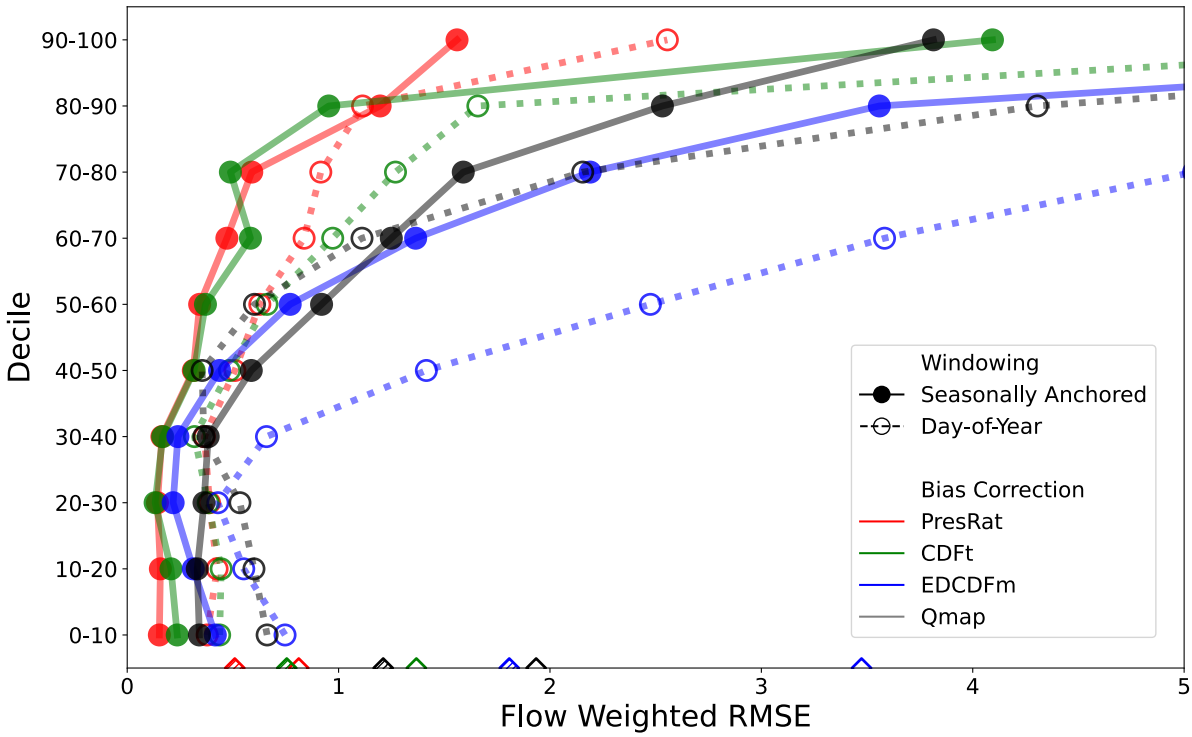

Fig. 8. Flow weighted root-mean-square error (RMSE) in the representation of model-predicted future change in mean flow at each decile averaged across the 6 streams. Solid (dotted) lines represent correction methods using seasonally anchored (standard day-of-year) windowing techniques. For solid (dotted) lines, the value of the flow weighted RMSE averaged across all deciles is indicated by a hatched (unfilled) triangle on the lower x-axis.

BC Method	Ensemble Mean RMSE Across Deciles [Flow Weighted %]
PresRat	0.51 (0.81)
CDFt	0.75 (1.37)
EDCDFm	1.81 (3.47)
Qmap	1.21 (1.93)

Table 4. Flow weighted root-mean-square error (RMSE) averaged over all deciles and across all streams. Methods using standard day-of-year windowing are shown in parentheses, and those using seasonally anchored are shown without parentheses.

568

569 *d. Temporal Shift in Peak Streamflow*

570 The previous sections focus on the ability of bias correction techniques to preserve
571 original model projected changes in the magnitude of annual and wet season flow. Because
572 the fingerprint of climate change for mountain rivers is characterized by changes in both
573 magnitude and timing of peak streamflow, we will now evaluate the ability of each correction
574 method and windowing technique to preserve projected shifts in seasonality. Using the
575 climatological milestone associated with the peak streamflow (defined in Section 4), we
576 compare the original model change (measured in days) in peak streamflow timing with the
577 bias corrected changes.

578 Evaluating the difference in Julian day of peak streamflow between the end-of-
579 century and historical periods, Figure 9 shows the original model change in days on the x-
580 axis and the change from the PresRat with seasonally anchored windowing method on the y-
581 axis for each of the 10 GCM-projected climates and 6 rivers. If the bias correction methods
582 preserve the original model signal exactly, all markers would fall on the dotted black 1-to-1
583 line. For the overwhelming majority of stream and GCM combinations, we see that the
584 temporal shift is well-preserved. Though the amount of change varies with GCM, it is most
585 strongly related to the how snow-dominated a watershed is over the historical period. The
586 largest signal of change is seen at New Melones (red markers), which loses its historical
587 snowmelt peak entirely. The snowiest basin, Millerton (green markers), doesn't exhibit as
588 large a signal because unlike New Melones, it retains a snowmelt peak in some projections.

589 Table 5 summarizes the preservation of the projected temporal shifts for the various
590 bias correction methods and windowing techniques. For the PresRat and CDFt methods,
591 which best preserve changes in streamflow magnitude, the seasonally anchored windowing
592 method yields similar error metrics as the standard day-of-year technique. By virtue of
593 locking windows to Julian days, the day-of-year method does a good job at preserving the
594 raw model signal of temporal change. Notably, the seasonally anchored method achieves the
595 same efficacy (for PresRat and CDFt) as the day-of-year method without requiring identical
596 windows for the historical and future datasets.

597

BC Method	R2	Ens. Mean Error [days]	RMSE [days]
PresRat	0.9 (0.9)	0.4 (0.1)	6.8 (6.9)
CDFt	0.9 (0.9)	0.1 (0.1)	7.1 (7.0)
EDCDFm	0.6 (0.9)	3.1 (-0.5)	15.3 (6.7)
Qmap	0.8 (0.9)	0.1 (0.4)	11.1 (7.6)

598 Table 5. Summary of the ability of each bias correction method and windowing technique to
599 preserve the original model signal in the temporal shift in climatological peak streamflow.
600 Methods using standard day-of-year windowing are shown in parentheses, and those using
601 seasonally anchored are shown without parentheses.

602

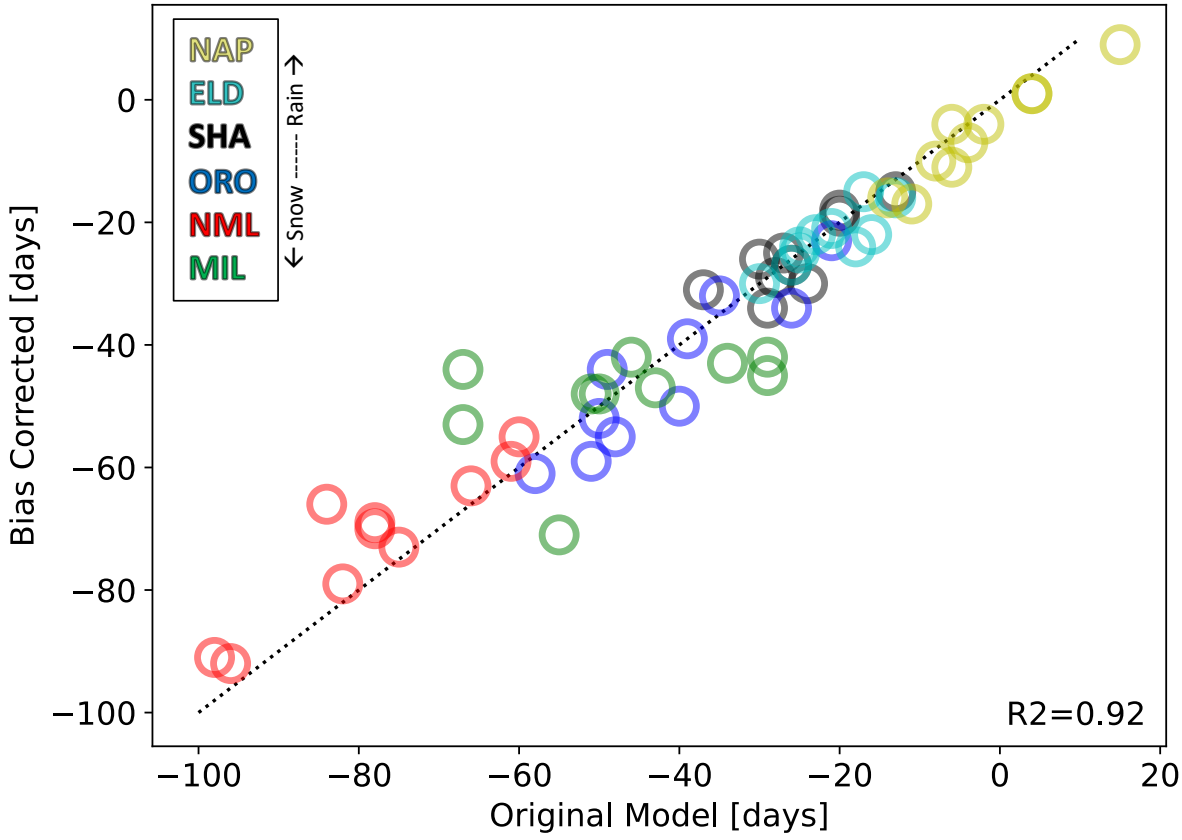

603

604 Fig. 9. Change in timing of peak climatological streamflow for the original model change (x-
605 axis) and PresRat with seasonally anchored windowing (y-axis) between the end-of-century

and historical periods. Markers represent the change for each GCM and are color-coded by stream. A dotted black 1-to-1 line is shown for reference.

6. Summary and Conclusion

Robust and reliable projections of changes in future streamflow are essential if we are to improve (or maintain) resilient water resources and mitigate damage to riparian ecosystems in the face of climate change. But raw simulations of streamflow are used in applications or impact models only at one's peril, unless first bias corrected. Traditional methods for bias correction operate by comparing future and historical model data from shared ranges of Julian days. However, the physical and environmental process that govern streamflow (or any hydrometeorological variable) are not necessarily fixed to calendar periods, especially in the context of climate change, which will advance melting season earlier in the year and can alter the seasonality of precipitation. In order to better connect the statistical process of bias correction to the underlying processes in hydrologic models, we introduce a novel windowing technique for bias correction of projected streamflows. Data are windowed based on hydrograph-relative time, not calendar day. By locating the temporal position of a given data point undergoing correction in relation to characteristic features of its average hydrograph (e.g., start of rising limb, peak flow, end of falling limb, minimum flow) we window data based on hydrographically-equivalent days across the observed, simulated-historical, and simulated-future periods.

We evaluate the efficacy of several bias correction methods, using both the standard day-of-year and our new seasonally anchored windowing technique, applied to streamflow projections for six California streams that range from rain- to snow dominated watersheds and that are responses to climate projections from a suite of 10 CMIP5 global climate models (GCMs) selected by the California Department of Water Resources as having good representation of the historical California hydroclimate. Based on the importance of individual high-magnitude streamflow events, total water year streamflow, and timing of peak flow on the natural and built environment, we argue that successful bias correction should accomplish three tasks: 1) preserve the water year mean climate change signal of the un-bias corrected flow projections, 2) preserve un-bias corrected changes at all quantiles, and 3) preserve any temporal signal of shifting seasonality in the un-bias corrected flow projections, all while correcting the simulated historical statistics to that of the observed

638 dataset. Evaluated as the percent difference relative to the historical period, we investigate the
639 degree to which the four bias methods and two windowing techniques preserve the un-bias
640 corrected signal of climate change across the study domain.
641 PresRat is the only bias correction method examined in this work that preserves the
642 original model, shorthand for hydrologic model output driven by downscaled and bias
643 corrected GCM data, signal of water year mean change and does so for both seasonally
644 anchored and standard day-of-year windowing techniques. Although the other 3 methods,
645 CDF transform (CDFt; Michelangeli et al., 2009), Equidistant CDF matching (EDCDFm; Li
646 et al., 2010), and Quantile Mapping (Qmap; Panofsky & Brier, 1968; Wood et al., 2002) do
647 not preserve the original model water year mean changes, even for these methods, seasonally
648 anchored windowing reduces the ensemble mean error by roughly a factor of two while
649 reducing the spread when compared to standard day-of-year windowing.
650 For an extreme and highly variable hydroclimate, like California, where a large
651 fraction of total water (both streamflow and precipitation) is contained in the top decile of the
652 distribution, it is vital that bias correction does not skew the original model projection signals
653 of change at the highest quantiles. Using the root-mean-square error evaluated at each decile
654 of wet season streamflow to gauge success, we find that 1) PresRat with seasonally anchored
655 windowing best preserves the raw signal at the top decile of flows, 2) PresRat with seasonally
656 anchored windowing best preserves the raw signal averaged over all deciles, and 3) using
657 seasonally anchored windowing improved the performance of each of the four bias correction
658 methods. These findings are true not only for the 10-member ensemble averaged over the six
659 streams, but true for all streams individually. With respect to streamflow magnitude,
660 regardless of their hydrological characteristics (e.g., rain- vs. snow dominated), the seasonally
661 anchored windowing technique was more effective in preserving the original model signals of
662 climate change.
663 Finally, because any shift in seasonality of snow-fed rivers will have strong impacts
664 on both the natural and built environments, we examine the extent to which bias correction
665 methods alter the original model signals of shifting seasons. We measure the change in
666 seasonality by finding the difference between the Julian dates coinciding with peak
667 streamflow in the simulated-future and simulated-historical periods. While the seasonally
668 anchored windowing technique improved the preservation of original model signals in
669 magnitude, we find that both windowing methods preserve the shift in seasonality equally

well (for PresRat and CDFt) with mean bias values < 1 day and root-mean-square error of ~7 days.

In summary, seasonally anchored windowing, as opposed to the standard day-of-year technique, yields better bias corrected projections of future streamflow across a subset of six streams ranging from rain- to snow- dominated ecosystems in California. Without sacrificing any capacity to preserve projected changes in timing of peak streamflow, the seasonally anchored method improves the preservation of magnitude changes in the un-bias corrected flow projections. This is true not only for the water year mean signal, which is important as it relates to the total volume of water flowing through the river over the course of the year, but is also true for both low and high streamflow events which have an outsized imprint on California's hydroclimate, water resources, and ecosystems.

While this work focused largely on wet season streamflow, Figure 10 highlights an important vulnerability of the standard day-of-year windowing concerning late season flows. Since biases from the early receding limb of the historical period hydrograph are applied to near-baseflow streamflow during the end-of-century period (because both occur over the same calendar-based period), the resulting bias corrected projections can represent something very unphysical: streamflow decreases past baseflow during the receding limb before rebounding and then receding once more until it reaches baseflow (dashed lines). In contrast, the future period hydrographs for seasonally anchored methods (solid lines) do not exhibit this unphysical behavior because they apply biases from equivalent stretches of the climatologies. Because this seasonal shift is driven by warming temperatures resulting in diminished snowpack whose peak volume is pushed earlier into the water year, this non-physical feature is most prevalent for historically snow-dominated watersheds.

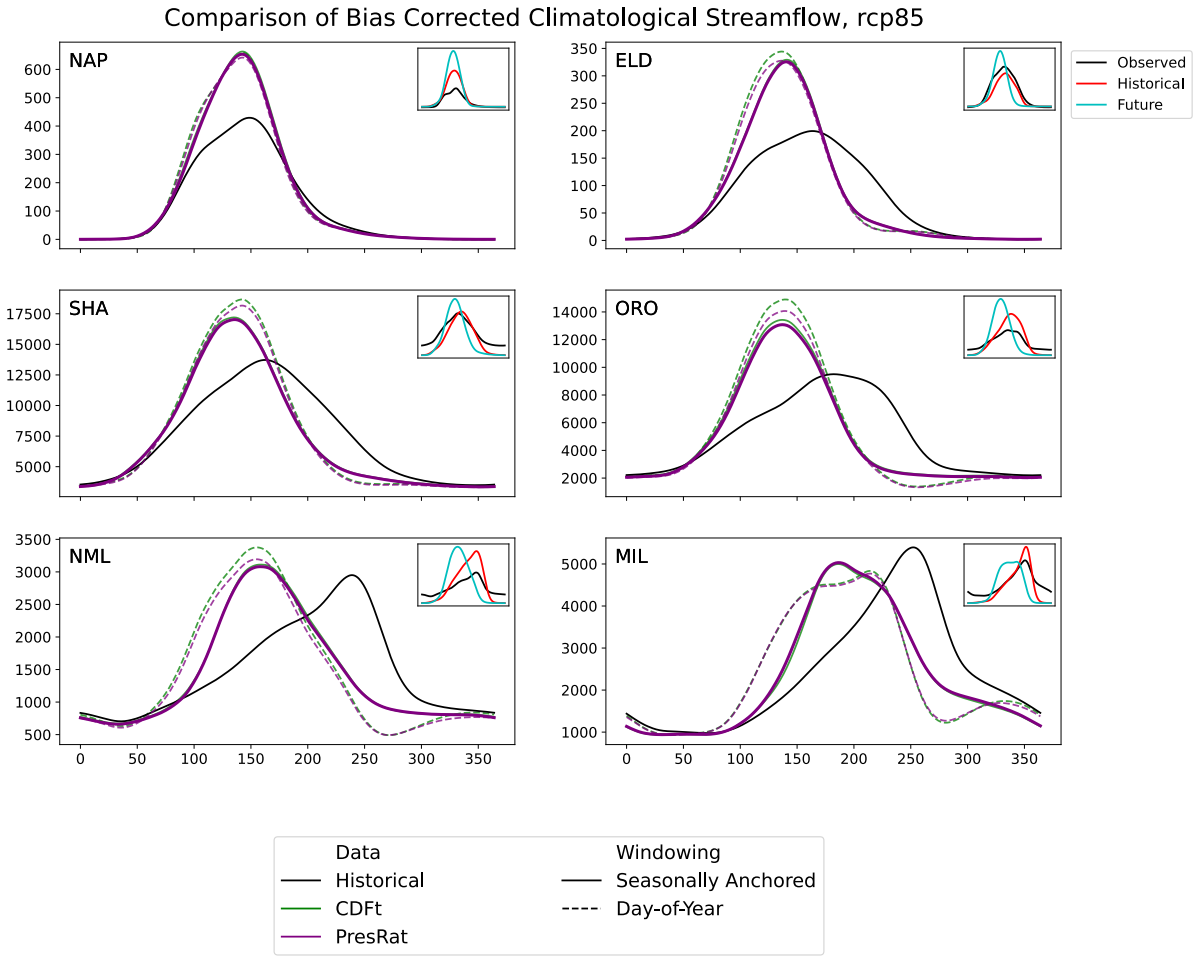

693

694 Fig. 10. Ensemble mean climatological hydrographs for raw and bias corrected data at each
695 of the 6 streams. The upper inlay depicts observed (black) and original model hydrographs of
696 the historical (red) and end-of-century (blue) periods for each river. The main subplots show
697 the bias corrected historical hydrograph (black) alongside end-of-century bias corrected
698 hydrographs for PresRat (purple) and CDFt (green) using seasonally anchored (solid) and
699 day-of-year (dashed) windowing methods.

700

701 This work 1) demonstrates the inability of bias correction with day-of-year
702 windowing to provide reliable projections of variables whose climate change signal is
703 characterized by changes in both magnitude and seasonality, and 2) introduces a novel
704 windowing method which moves towards 'process informed' bias correction wherein
705 environmental and physical processes, rather than calendar dates, are shared by windowed
706 data. Given the importance of streamflow projections in creating more resilient water
707 resources, it may be pertinent to evaluate the difference in future streamflow projections

across a wider range of California rivers using both seasonally anchored and day-of-year windowing methods. Although we conceptualized and applied the method for the purpose of bias correcting streamflow in California, the fundamental technique of windowing based on the position (in time) of a given data point in reference to some climatological milestones could be applied to variables other than streamflow (e.g., snow water equivalent, which is also expected to have a significant seasonal shift in the future). For variables that will have seasonal shifts in the future, it is important to move towards 'process informed' bias correction and away from calendar-based methods that are completely detached from the physical processes governing the systems. Although the method introduced here does not directly tether the statistical process of bias correction to the underlying physics of GCMs or land surface models, it is a step in the appropriate direction.

Acknowledgments.

All authors were supported by the CA Department of Water Resources grant number 4600013361. MDS received support from the US Army Corps of Engineers, grant number USACE W912HZ-19-SOI-002. DWP received support from the California Energy Commission grants EPC-16-063, PIR-19-007, and EPC-20-006 and NOAA's RISA California-Nevada Climate Applications Program Award NA17OAR4310284.

Data Availability Statement.

The data generated in this study will be available at [currently working on obtaining a DOI for the data].

APPENDIX

Appendix A: Identification of Peak Streamflow Milestone for Bimodal Climatological Hydrographs

Section 4.1.b describes the process of selecting peak streamflow milestones. While the vast majority of climatological hydrographs assessed in this study are not bimodal, for some future projections of historically snow-dominated rivers, the climatological hydrograph contains two local maxima (Figure A1). Recall that the purpose of the seasonally anchored

738 windowing technique is to conduct bias correction across data with similar background
739 physical and environmental processes. The peak milestone in the historical period
740 corresponds to streamflow generated from snowmelt. The future period bimodal hydrograph
741 is characterized by what is likely an earlier rain-dominated peak and a later-season snowmelt-
742 dominated peak. Although the rain-dominated peak may be higher in magnitude, we select
743 the later, snowmelt peak for the location of the milestone to better ensure that the data used in
744 the bias correction shares similar physical and environmental processes.

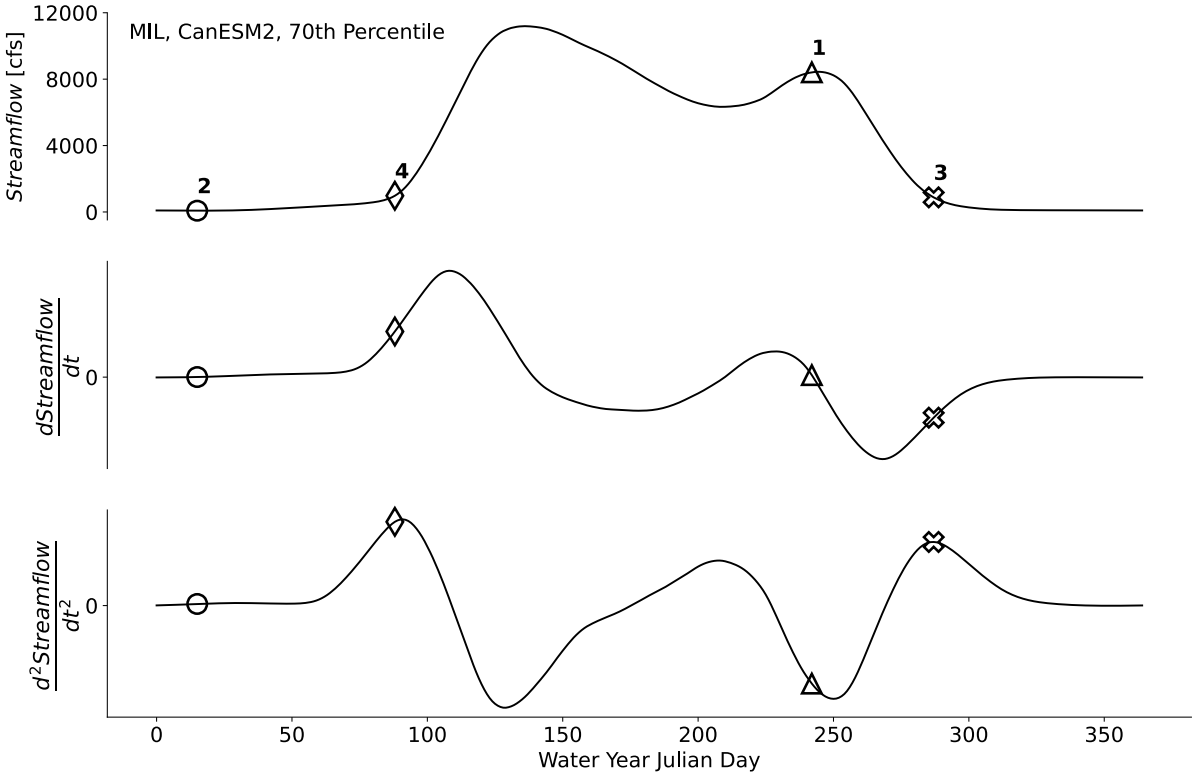

745

746 Fig. A1. Visual depiction of the algorithm used to identify climatological milestones for the
747 seasonally anchored windowing method for the special case of bimodal hydrographs. End-of-
748 century climatological data from the Millerton/Friant Dam stream and CanESM2 GCM is
749 shown at the 70th percentile to illustrate the method. Daily mean climatological streamflow
750 (top), and the first and second derivatives of streamflow with respect to time (middle and
751 bottom respectively) are plotted on against water year Julian day. Numerical annotation is
752 used to indicate the workflow by which the four seasonal milestones are assigned: (1) Peak
753 streamflow (triangle), (2) Minimum streamflow (circle), (3) Start of the dry season/end of
754 receding limb (x), and (4) Start of the wet season/beginning of the rising limb (diamond).
755 Note that the peak milestone (triangle), is not associated with the true maximum value of
756 streamflow, but rather with the local maximum during the snowmelt period.

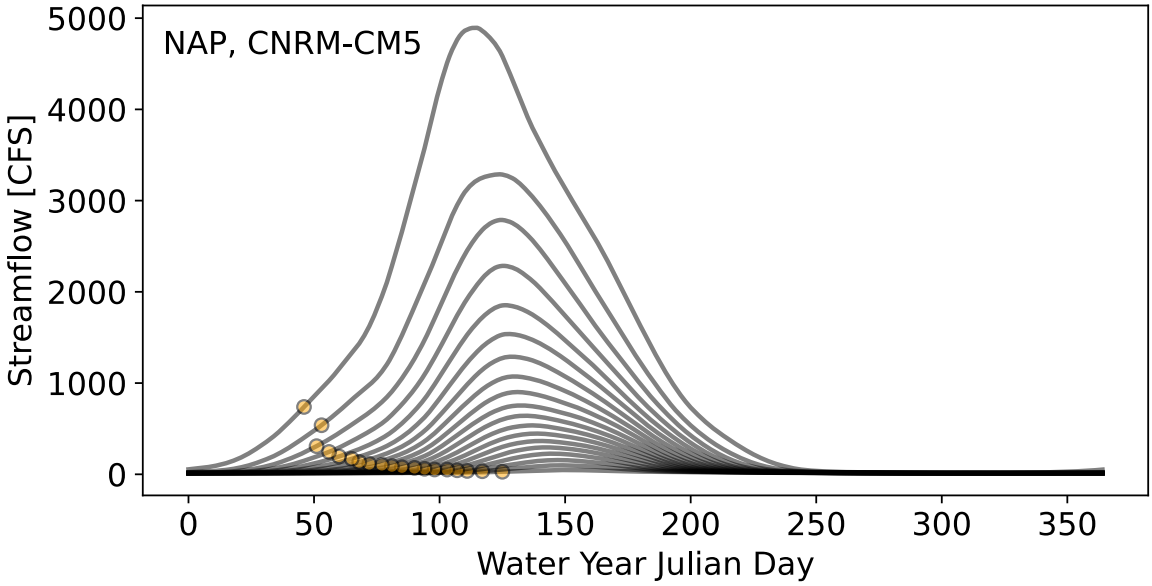

Fig. A2. Climatological hydrographs (lines) for flows ranging from the 5th to 95th percentile by intervals of 5 percentage points. Here, we see how the location of the 'start of wet season' milestone (circle) varies as a function of quantile.

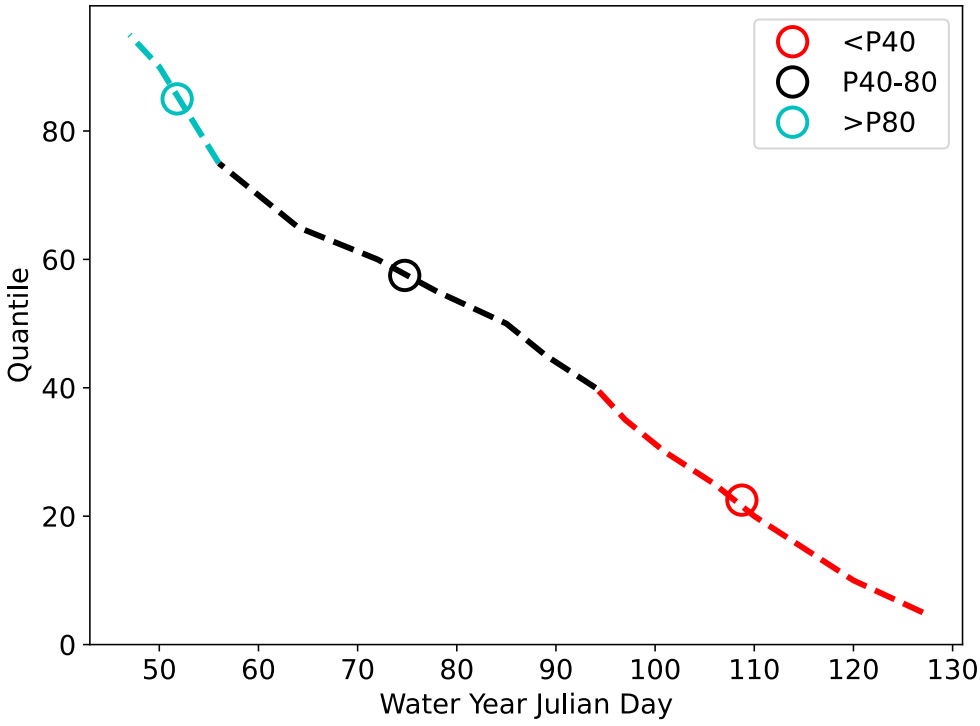

764 Fig. A3. Day of water year associated with the 'start of wet season' milestone (from Fig. A2)
765 for flows below 40th percentile (red), 40th-80th percentile (black), and above 80th percentile
766 (blue). The mean value over each respective range is indicated by a circle.

767

768

769 **Appendix B: Original model Change in Wet Season Streamflow by Decile**

770 In accompaniment of Figure 6 in section 5.c, Appendix B provides the original model
771 signal in wet season streamflow change by decile for the remaining 5 rivers.

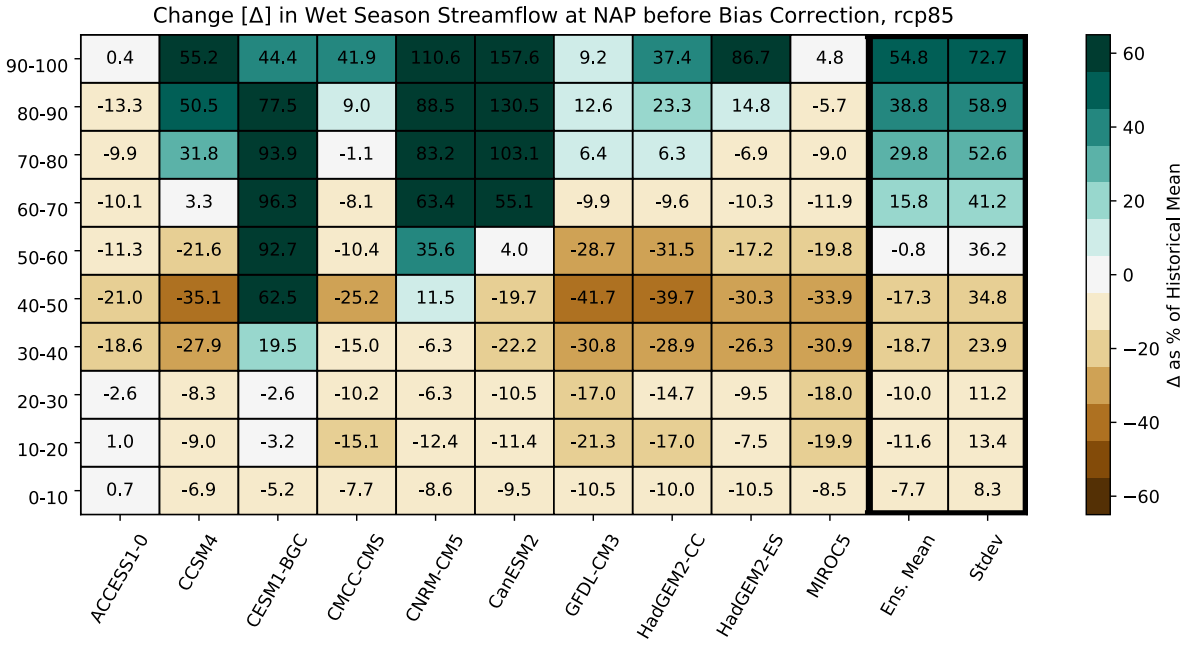

772

773 Fig. B1. Original model projected change in Napa River streamflow by decile (rows) and
774 GCM (columns) with the 10-member ensemble mean and standard deviation (farthest right
775 columns). Using units of 'percent change from the historical mean', increasing streamflow is
776 indicated by green color-shading, and decreasing streamflow by brown. Values under 5%
777 change appear as white.

778

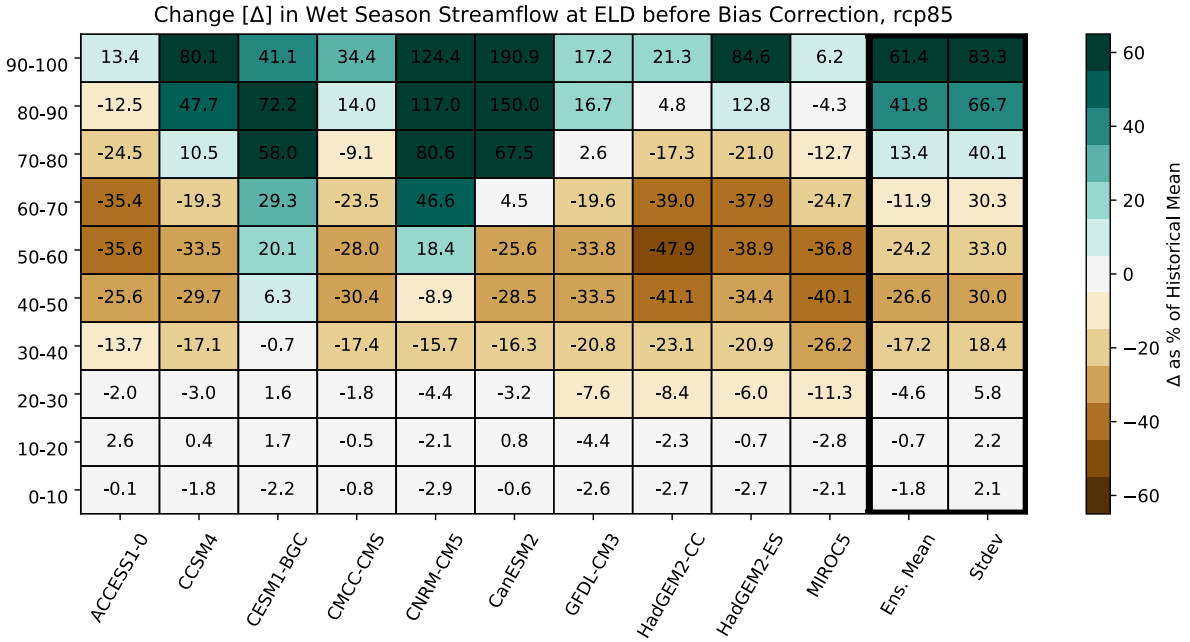

779

780 Fig. B2. Original model projected change in Elder Creek streamflow by decile (rows) and
781 GCM (columns) with the 10-member ensemble mean and standard deviation (farthest right
782 columns). Using units of 'percent change from the historical mean', increasing streamflow is
783 indicated by green color-shading, and decreasing streamflow by brown. Values under 5%
784 change appear as white.

785

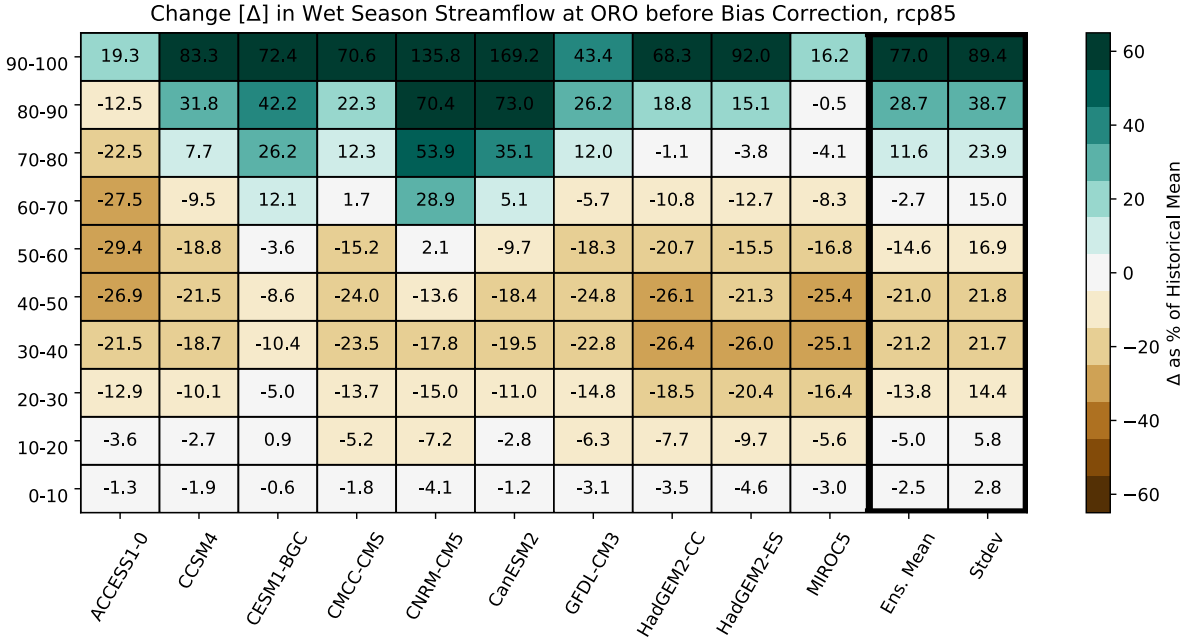

786

787 Fig. B3. Original model projected change in Oroville Dam streamflow by decile (rows) and
788 GCM (columns) with the 10-member ensemble mean and standard deviation (farthest right
789 columns). Using units of 'percent change from the historical mean', increasing streamflow is
790 indicated by green color-shading, and decreasing streamflow by brown. Values under 5%
791 change appear as white.

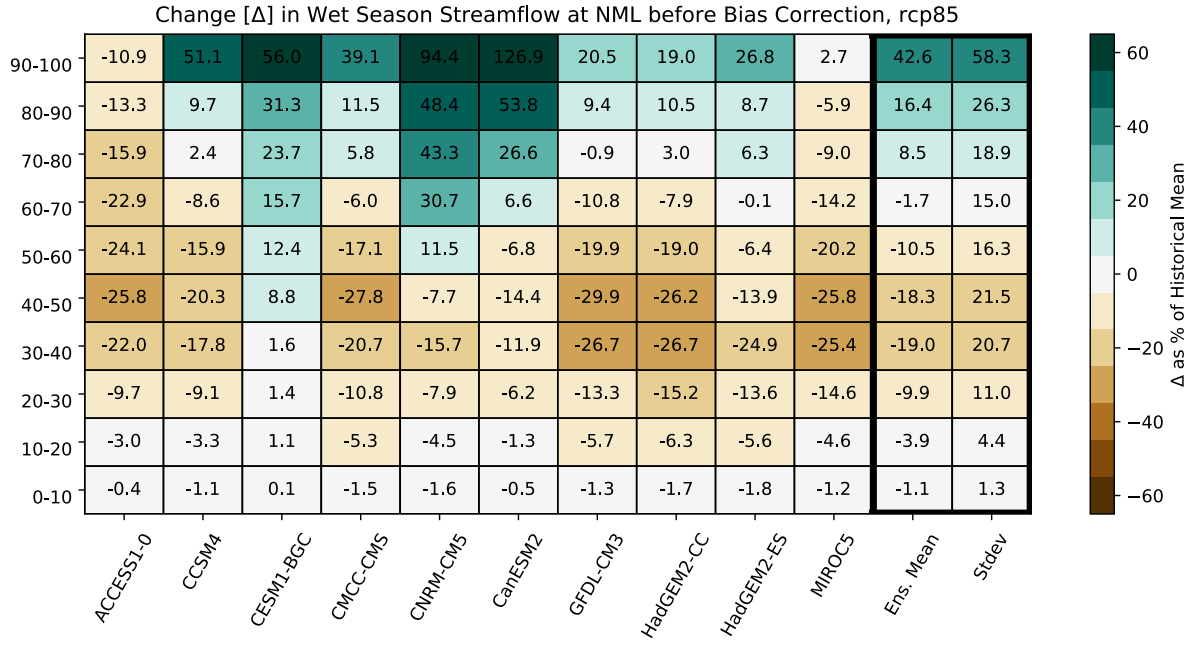

792

793 Fig. B4. Original model projected change in New Melones Reservoir streamflow by decile
794 (rows) and GCM (columns) with the 10-member ensemble mean and standard deviation
795 (farthest right columns). Using units of 'percent change from the historical mean', increasing
796 streamflow is indicated by green color-shading, and decreasing streamflow by brown. Values
797 under 5% change appear as white.

798

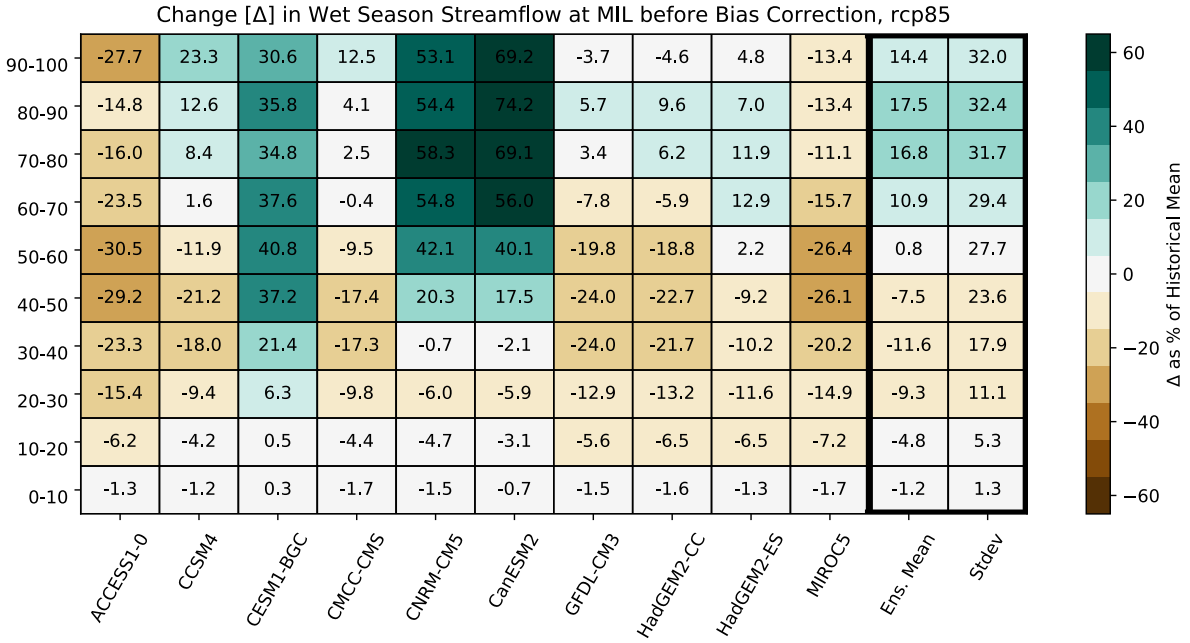

799

800 Fig. B5. Original model projected change in Millerton/Friant Dam streamflow by decile
801 (rows) and GCM (columns) with the 10-member ensemble mean and standard deviation
802 (farthest right columns). Using units of 'percent change from the historical mean', increasing
803 streamflow is indicated by green color-shading, and decreasing streamflow by brown. Values
804 under 5% change appear as white.

805

806 **Appendix C: Error in Wet Season Streamflow by Decile**

807 In accompaniment of Figure 7 in section 5.c, Appendix C provides the error in wet
808 season streamflow change by decile for the remaining combinations of bias correction and
809 windowing techniques.

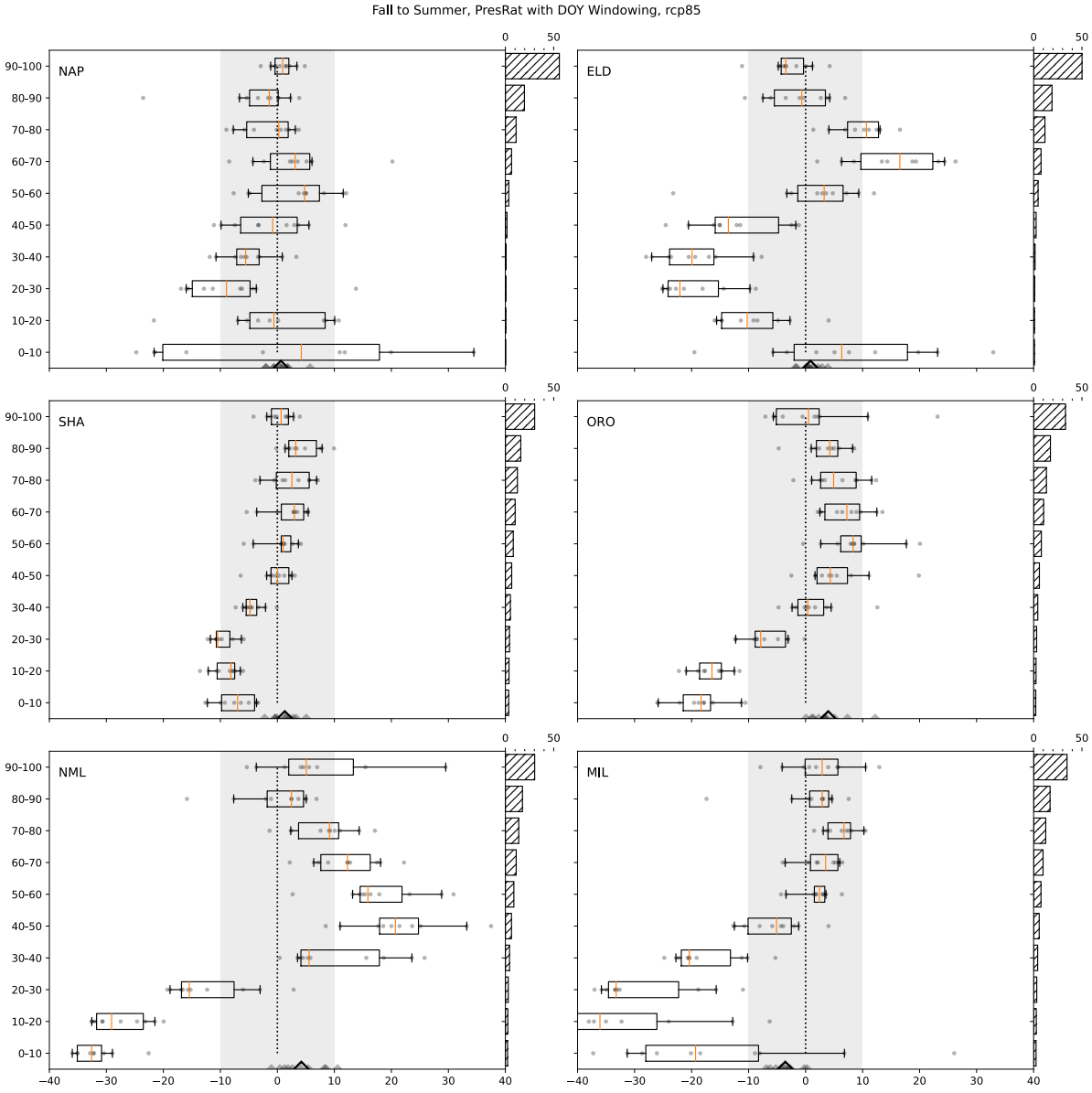

Fig. C1. Error by decile for change in wet season streamflow for PresRat with standard day-of-year windowing. Errors (x-axis) for individual GCMs are depicted by grey circles, the mean error across the 10-member ensemble is depicted by an orange line. The box edges and whiskers represent the middle 5 and 8 GCMs respectively. The error for a single GCM averaged over all deciles is depicted as a small grey triangle on the x-axis and the value for the 10-member ensemble mean is denoted by a large triangle. For reference, the grey shading and dashed black line correspond to ± 10% error and 0% error respectively. For each stream, the right y-axis depicts the historical percentage of total wet season streamflow contained in each decile averaged across the 10-member ensemble. Subplots are organized so that as you move down the rows, streams transition from rain- to snow dominated over the historical period.

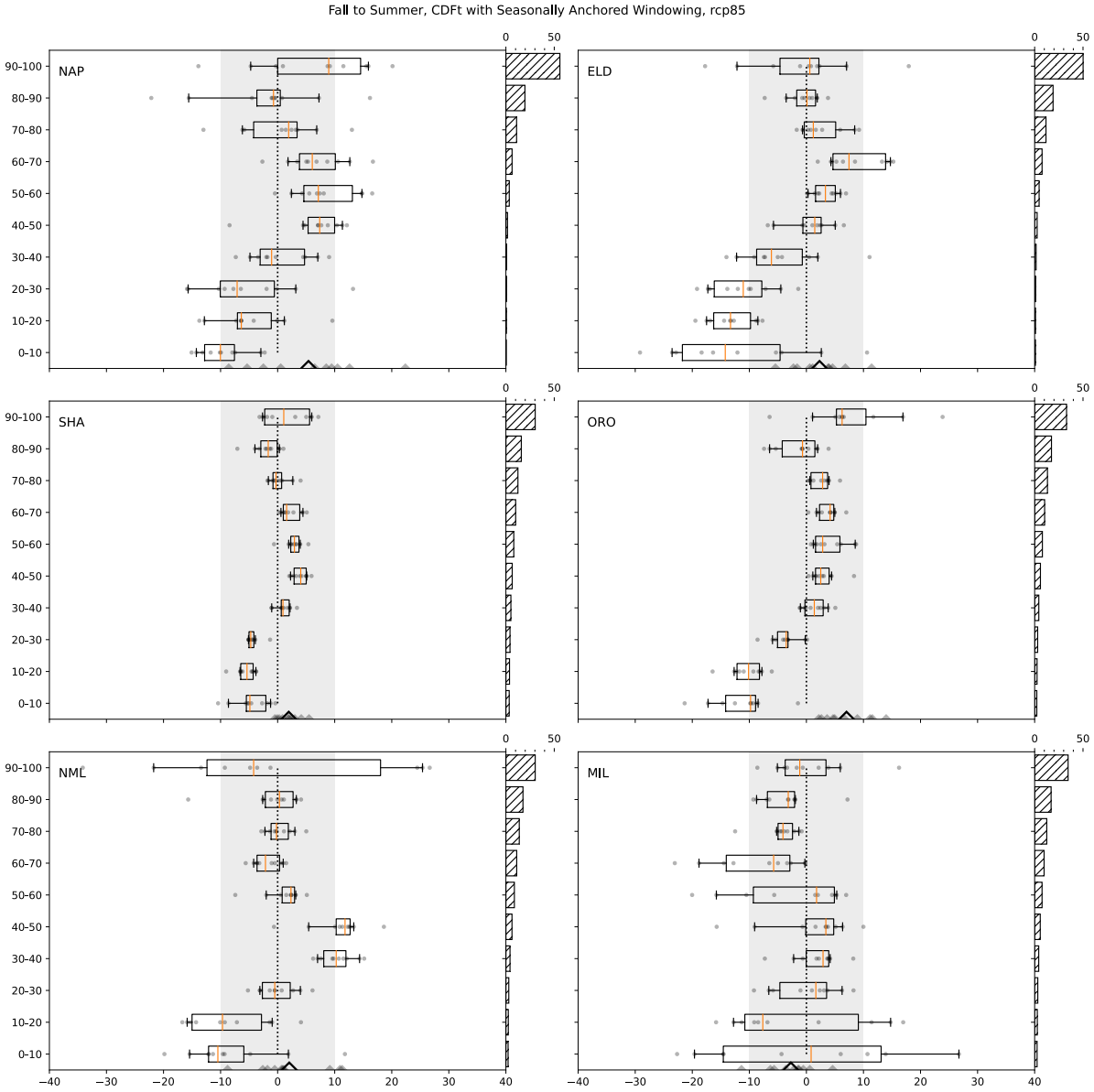

Fig. C2. Error by decile for change in wet season streamflow for CDFt with seasonally anchored windowing. Errors (x-axis) for individual GCMs are depicted by grey circles, the mean error across the 10-member ensemble is depicted by an orange line. The box edges and whiskers represent the middle 5 and 8 GCMs respectively. The error for a single GCM averaged over all deciles is depicted as a small grey triangle on the x-axis and the value for the 10-member ensemble mean is denoted by a large triangle. For reference, the grey shading and dashed black line correspond to ± 10% error and 0% error respectively. For each stream, the right y-axis depicts the historical percentage of total wet season streamflow contained in each decile averaged across the 10-member ensemble. Subplots are organized so that as you move down the rows, streams transition from rain- to snow dominated over the historical period.

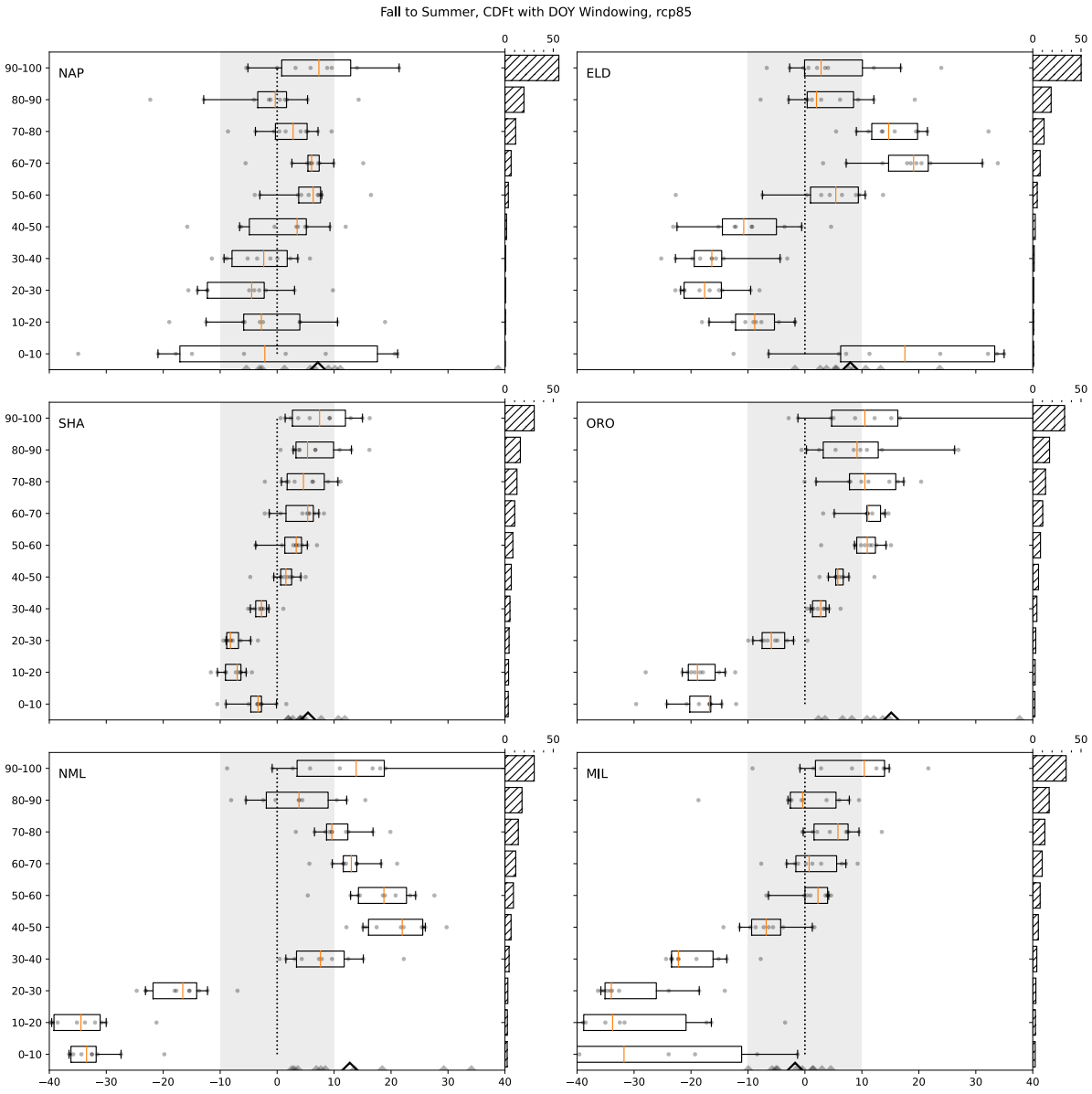

Fig. C3. Error by decile for change in wet season streamflow for CDFt with standard day-of-year windowing. Errors (x-axis) for individual GCMs are depicted by grey circles, the mean error across the 10-member ensemble is depicted by an orange line. The box edges and whiskers represent the middle 5 and 8 GCMs respectively. The error for a single GCM averaged over all deciles is depicted as a small grey triangle on the x-axis and the value for the 10-member ensemble mean is denoted by a large triangle. For reference, the grey shading and dashed black line correspond to ± 10% error and 0% error respectively. For each stream, the right y-axis depicts the historical percentage of total wet season streamflow contained in each decile averaged across the 10-member ensemble. Subplots are organized so that as you move down the rows, streams transition from rain- to snow dominated over the historical period.

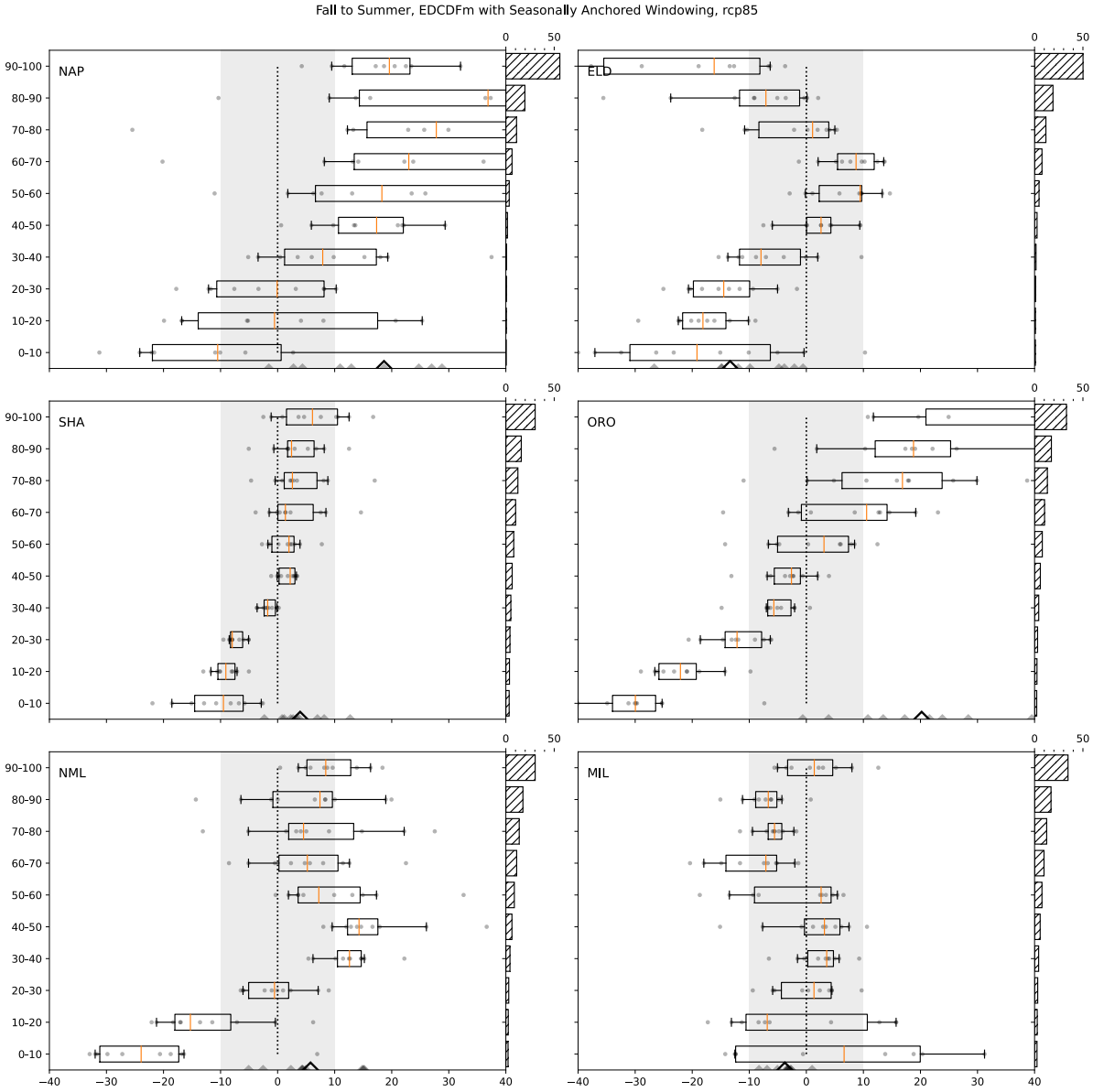

Fig. C4. Error by decile for change in wet season streamflow for EDCDFm with seasonally anchored windowing. Errors (x-axis) for individual GCMs are depicted by grey circles, the mean error across the 10-member ensemble is depicted by an orange line. The box edges and whiskers represent the middle 5 and 8 GCMs respectively. The error for a single GCM averaged over all deciles is depicted as a small grey triangle on the x-axis and the value for the 10-member ensemble mean is denoted by a large triangle. For reference, the grey shading and dashed black line correspond to ± 10% error and 0% error respectively. For each stream, the right y-axis depicts the historical percentage of total wet season streamflow contained in each decile averaged across the 10-member ensemble. Subplots are organized so that as you move down the rows, streams transition from rain- to snow dominated over the historical period.

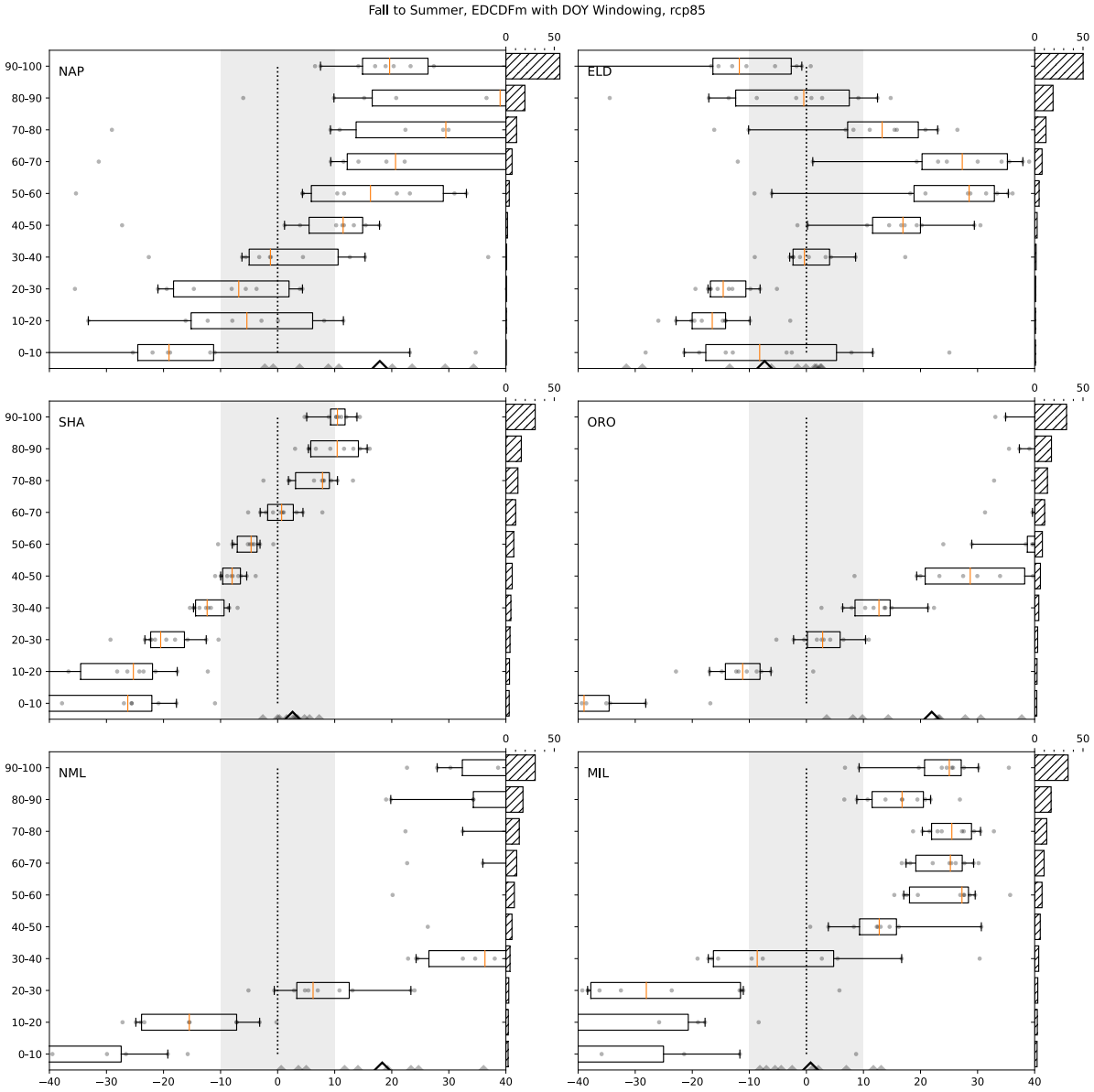

Fig. C5. Error by decile for change in wet season streamflow for EDCDFm with standard day-of-year windowing. Errors (x-axis) for individual GCMs are depicted by grey circles, the mean error across the 10-member ensemble is depicted by an orange line. The box edges and whiskers represent the middle 5 and 8 GCMs respectively. The error for a single GCM averaged over all deciles is depicted as a small grey triangle on the x-axis and the value for the 10-member ensemble mean is denoted by a large triangle. For reference, the grey shading and dashed black line correspond to ± 10% error and 0% error respectively. For each stream, the right y-axis depicts the historical percentage of total wet season streamflow contained in each decile averaged across the 10-member ensemble. Subplots are organized so that as you move down the rows, streams transition from rain- to snow dominated over the historical period.

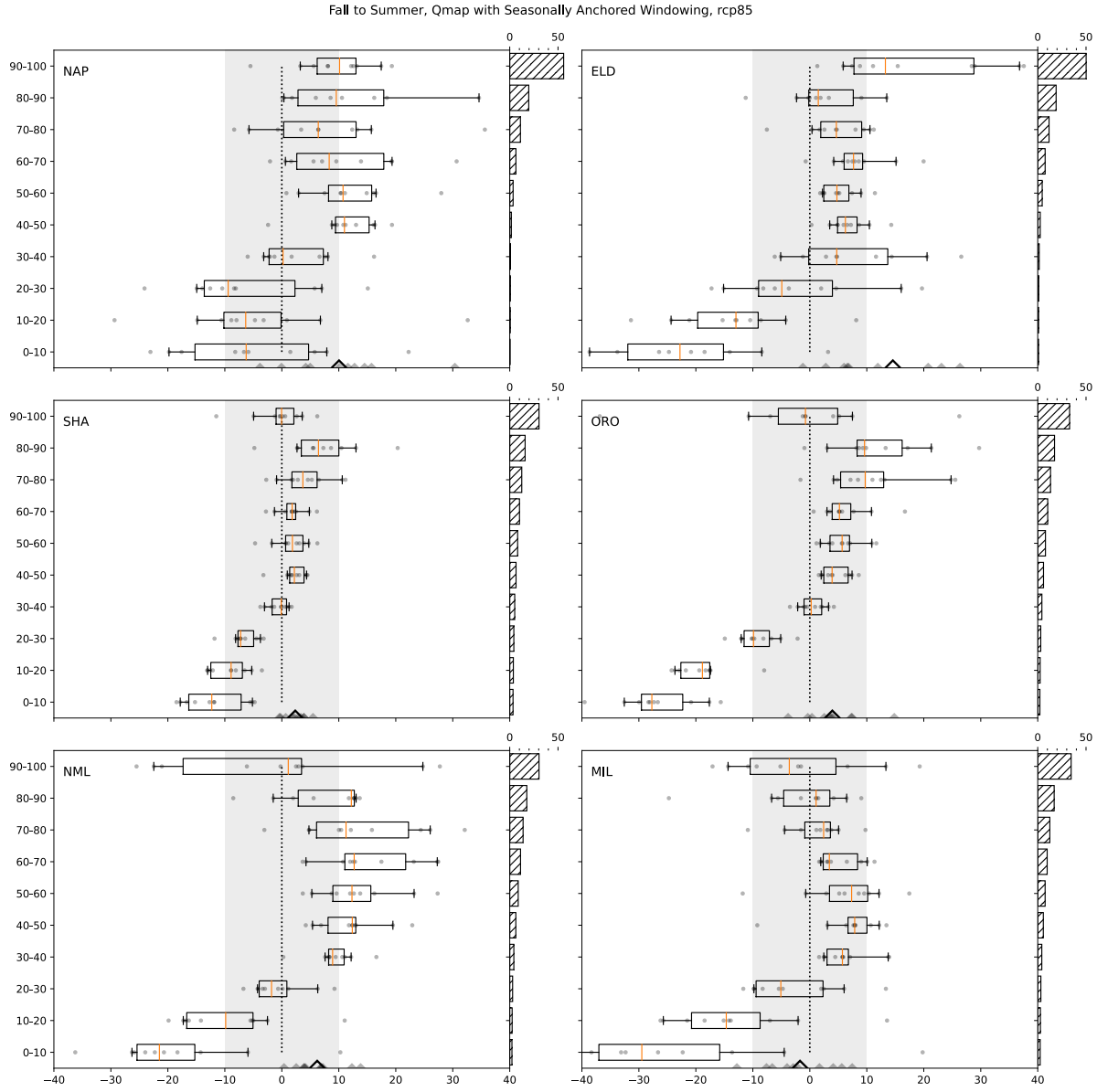

Fig. C6. Error by decile for change in wet season streamflow for Qmap with seasonally anchored windowing. Errors (x-axis) for individual GCMs are depicted by grey circles, the mean error across the 10-member ensemble is depicted by an orange line. The box edges and whiskers represent the middle 5 and 8 GCMs respectively. The error for a single GCM averaged over all deciles is depicted as a small grey triangle on the x-axis and the value for the 10-member ensemble mean is denoted by a large triangle. For reference, the grey shading and dashed black line correspond to ± 10% error and 0% error respectively. For each stream, the right y-axis depicts the historical percentage of total wet season streamflow contained in each decile averaged across the 10-member ensemble. Subplots are organized so that as you move down the rows, streams transition from rain- to snow dominated over the historical period.

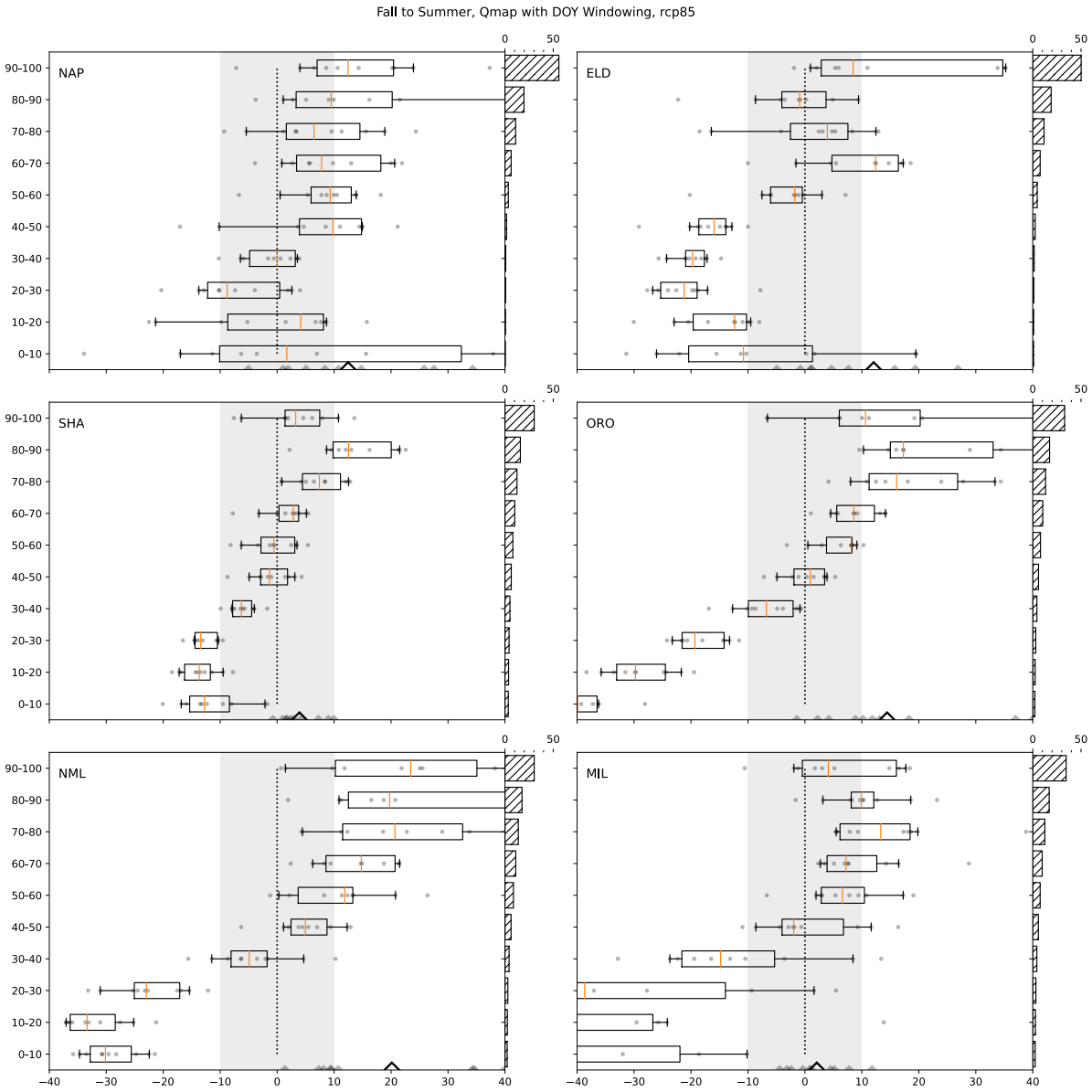

Fig. C7. Error by decile for change in wet season streamflow for Qmap with standard day-of-year windowing. Errors (x-axis) for individual GCMs are depicted by grey circles, the mean error across the 10-member ensemble is depicted by an orange line. The box edges and whiskers represent the middle 5 and 8 GCMs respectively. The error for a single GCM averaged over all deciles is depicted as a small grey triangle on the x-axis and the value for the 10-member ensemble mean is denoted by a large triangle. For reference, the grey shading and dashed black line correspond to ± 10% error and 0% error respectively. For each stream, the right y-axis depicts the historical percentage of total wet season streamflow contained in each decile averaged across the 10-member ensemble. Subplots are organized so that as you move down the rows, streams transition from rain- to snow dominated over the historical period.

894

895 REFERENCES

896 Barnett, T. P., & Pierce, D. W. (2009). Sustainable water deliveries from the Colorado River
897 in a changing climate. *Proceedings of the National Academy of Sciences of the United*
898 *States of America*, *106*(18), 7334–7338. https://doi.org/10.1073/pnas.0812762106

899 California Department of Water Resources Climate Change Technical Advisory Group.
900 (2015). *Perspectives and Guidance for Climate Change Analysis*. Retrieved from
901 http://www.water.ca.gov/climatechange/docs/2015/Perspectives_Guidance_Climate_Ch
902 ange_Analysis.pdf

903 Cayan, D. R., Kammerdiener, S. A., Dettinger, M. D., Caprio, J. M., & Peterson, D. H.
904 (2001). Changes in the Onset of Spring in the Western United States. *Bulletin of the*
905 *American Meteorological Society*, *82*(3), 399–415. https://doi.org/10.1175/1520-
906 0477(2001)082<0399:CITOOS>2.3.CO;2

907 Das, T., Pierce, D. W., Cayan, D. R., Vano, J. A., & Lettenmaier, D. P. (2011). The
908 importance of warm season warming to western U.S. streamflow changes. *Geophysical*
909 *Research Letters*, *38*(23), 1–5. https://doi.org/10.1029/2011GL049660

910 Dettinger, M. D., Ralph, F. M., Das, T., Neiman, P. J., & Cayan, D. R. (2011). Atmospheric
911 Rivers, Floods and the Water Resources of California. *Water*, *3*(2), 445–478.
912 https://doi.org/10.3390/w3020445

913 Fowler, H. J., Blenkinsop, S., & Tebaldi, C. (2007). Linking climate change modelling to
914 impacts studies: recent advances in downscaling techniques for hydrological modelling.
915 *International Journal of Climatology*, *27*(12), 1547–1578.
916 https://doi.org/10.1002/joc.1556

917 Gershunov, A., Shulgina, T., Clemesha, R. E. S., Guirguis, K., Pierce, D. W., Dettinger, M.
918 D., … Ralph, F. M. (2019). Precipitation regime change in Western North America: The
919 role of Atmospheric Rivers. *Scientific Reports*, *9*(1), 1–11.
920 https://doi.org/10.1038/s41598-019-46169-w

921 Gonzalez, P. (U. S. N. P. S., Garfin, G. M. (University of A., Breshears, D. D., Brooks, K.
922 M., Brown, H. E., Elias, E. H., … Udal, B. H. (2018). Fourth National Climate
923 Assessment: Southwest. *Impacts, Risks, and Adaptation in the United States: Fourth*

National Climate Assessment, *II*, 1101–1184. https://doi.org/10.7930/NCA4.2018.CH25

Gudmundsson, L., Bremnes, J. B., Haugen, J. E., & Engen-Skaugen, T. (2012). Technical Note: Downscaling RCM precipitation to the station scale using statistical transformations – a comparison of methods. *Hydrology and Earth System Sciences*, *16*(9), 3383–3390. https://doi.org/10.5194/hess-16-3383-2012

Hagemann, S., Chen, C., Haerter, J. O., Heinke, J., Gerten, D., & Piani, C. (2011). Impact of a statistical bias correction on the projected hydrological changes obtained from three GCMs and two hydrology models. *Journal of Hydrometeorology*, *12*(4), 556–578. https://doi.org/10.1175/2011JHM1336.1

He, M., Anderson, M., Schwarz, A., Das, T., Lynn, E., Anderson, J., … Arnold, W. (2019). Potential changes in runoff of California's major water supply watersheds in the 21st century. *Water (Switzerland)*, *11*(8). https://doi.org/10.3390/w11081651

Hewitson, B. C., Daron, J., Crane, R. G., Zermoglio, M. F., & Jack, C. (2014). Interrogating empirical-statistical downscaling. *Climatic Change*, *122*(4), 539–554. https://doi.org/10.1007/s10584-013-1021-z

Hill, M. T., Platts, W. S., & Beschta, R. L. (1991). Ecological and geomorphological concepts for instream and out-of- channel flow requirements. *Rivers*, *2*(3), 198–210.

Huning, L. S., & AghaKouchak, A. (2018). Mountain snowpack response to different levels of warming. *Proceedings of the National Academy of Sciences of the United States of America*, *115*(43), 10932–10937. https://doi.org/10.1073/pnas.1805953115

Kalra, A., Piechota, T. C., Davies, R., & Tootle, G. A. (2008). Changes in U.S. Streamflow and Western U.S. Snowpack. *Journal of Hydrologic Engineering*, *13*(3), 156–163. https://doi.org/10.1061/(asce)1084-0699(2008)13:3(156)

Knowles, N., Cronkite-Ratcliff, C., Pierce, D. W., & Cayan, D. R. (2018). Responses of Unimpaired Flows, Storage, and Managed Flows to Scenarios of Climate Change in the San Francisco Bay-Delta Watershed. *Water Resources Research*, *54*(10), 7631–7650. https://doi.org/10.1029/2018WR022852

Knowles, Noah, & Cronkite-Ratcliff, C. (2018). *Modeling Managed Flows in the Sacramento/San Joaquin Watershed, California, Under Scenarios of Future Change for CASCaDE2*. 1–38. https://doi.org/https://doi.org/10.3133/ofr20181101

954 Li, H., Sheffield, J., & Wood, E. F. (2010). Bias correction of monthly precipitation and
955 temperature fields from Intergovernmental Panel on Climate Change AR4 models using
956 equidistant quantile matching. *Journal of Geophysical Research Atmospheres*, *115*(10).
957 https://doi.org/10.1029/2009JD012882

958 Liang, X., Lettenmaier, D. P., Wood, E. F., & Burges, S. J. (1994). A simple hydrologically
959 based model of land surface water and energy fluxes for general circulation models.
960 *Journal of Geophysical Research*. https://doi.org/10.1029/94jd00483

961 Maraun, D. (2013). Bias correction, quantile mapping, and downscaling: Revisiting the
962 inflation issue. *Journal of Climate*, *26*(6), 2137–2143. https://doi.org/10.1175/JCLI-D-
963 12-00821.1

964 Maraun, D., Shepherd, T. G., Widmann, M., Zappa, G., Walton, D., Gutiérrez, J. M., …
965 Mearns, L. O. (2017). Towards process-informed bias correction of climate change
966 simulations. *Nature Climate Change*, *7*(11), 764–773.
967 https://doi.org/10.1038/nclimate3418

968 Maurer, E. P., & Pierce, D. W. (2014). Bias correction can modify climate model simulated
969 precipitation changes without adverse effect on the ensemble mean. *Hydrology and*
970 *Earth System Sciences*, *18*(3), 915–925. https://doi.org/10.5194/hess-18-915-2014

971 Michelangeli, P. A., Vrac, M., & Loukos, H. (2009). Probabilistic downscaling approaches:
972 Application to wind cumulative distribution functions. *Geophysical Research Letters*,
973 *36*(11), 2–7. https://doi.org/10.1029/2009GL038401

974 Mioduszewski, J. R., Rennermalm, A. K., Robinson, D. A., & Wang, L. (2015). Controls on
975 spatial and temporal variability in Northern Hemisphere terrestrial snow melt timing,
976 1979-2012. *Journal of Climate*, *28*(6), 2136–2153. https://doi.org/10.1175/JCLI-D-14-
977 00558.1

978 Mote, P. W., Hamlet, A. F., Clark, M. P., & Lettenmaier, D. P. (2005). DECLINING
979 MOUNTAIN SNOWPACK IN WESTERN NORTH AMERICA*. *Bulletin of the*
980 *American Meteorological Society*, *86*(1), 39–50. https://doi.org/10.1175/BAMS-86-1-39

981 Mote, P. W., Li, S., Lettenmaier, D. P., Xiao, M., & Engel, R. (2018). Dramatic declines in
982 snowpack in the western US. *Npj Climate and Atmospheric Science*, *1*(1).
983 https://doi.org/10.1038/s41612-018-0012-1

984 Panofsky, H. A., & Brier, G. W. (1968). Some Applications of Statistics to Meteorology. In
985 *College of Mineral Industries, The Pennsylvania State University*.

986 Patterson, N. K., Lane, B. A., Sandoval-Solis, S., Pasternack, G. B., Yarnell, S. M., & Qiu, Y.
987 (2020). A hydrologic feature detection algorithm to quantify seasonal components of
988 flow regimes. *Journal of Hydrology*, *585*(August 2019), 124787.
989 https://doi.org/10.1016/j.jhydrol.2020.124787

990 Pederson, G. T., Gray, S. T., Ault, T., Marsh, W., Fagre, D. B., Bunn, A. G., … Graumlich,
991 L. J. (2011). Climatic controls on the snowmelt hydrology of the northern Rocky
992 Mountains. *Journal of Climate*, *24*(6), 1666–1687.
993 https://doi.org/10.1175/2010JCLI3729.1

994 Petts, G. E. (1996). Water Allocation to Protect River Ecosystems. *Regulated Rivers:*
995 *Research & Management*, *12*(4–5), 353–365. https://doi.org/10.1002/(SICI)1099-
996 1646(199607)12:4/5<353::AID-RRR425>3.0.CO;2-6

997 Pierce, D. W., & Cayan, D. R. (2013). The uneven response of different snow measures to
998 human-induced climate warming. *Journal of Climate*, *26*(12), 4148–4167.
999 https://doi.org/10.1175/JCLI-D-12-00534.1

1000 Pierce, D. W., Cayan, D. R., Maurer, E. P., Abatzoglou, J. T., & Hegewisch, K. C. (2015).
1001 Improved bias correction techniques for hydrological simulations of climate change.
1002 *Journal of Hydrometeorology*, *16*(6), 2421–2442. https://doi.org/10.1175/JHM-D-14-
1003 0236.1

1004 Pierce, D. W., Cayan, D. R., & Thrasher, B. L. (2014). Statistical downscaling using
1005 localized constructed analogs (LOCA). *Journal of Hydrometeorology*, *15*(6), 2558–
1006 2585. https://doi.org/10.1175/JHM-D-14-0082.1

1007 Pierce, D. W., Das, T., Cayan, D. R., Maurer, E. P., Miller, N. L., Bao, Y., … Tyree, M.
1008 (2013). Probabilistic estimates of future changes in California temperature and
1009 precipitation using statistical and dynamical downscaling. *Climate Dynamics*, *40*(3–4),
1010 839–856. https://doi.org/10.1007/s00382-012-1337-9

1011 Poff, N. L. R., Allan, J. D., Bain, M. B., Karr, J. R., Prestegaard, K. L., Richter, B. D., …
1012 Stromberg, J. C. (1997). The natural flow regime: A paradigm for river conservation and
1013 restoration. *BioScience*, *47*(11), 769–784. https://doi.org/10.2307/1313099

1014 Rajagopalan, B., Nowak, K., Prairie, J., Hoerling, M., Harding, B., Barsugli, J., … Udall, B.
1015 (2009). Water supply risk on the Colorado River: Can management mitigate? *Water*
1016 *Resources Research*, *45*(8), 1–7. https://doi.org/10.1029/2008WR007652

1017 Richter, B. D., Baumgartner, J. V., Powell, J., & Braun, D. P. (1996). A Method for
1018 Assessing Hydrologic Alteration within Ecosystems. *Conservation Biology*, *10*(4),
1019 1163–1174. https://doi.org/10.1046/j.1523-1739.1996.10041163.x

1020 Salathé, E. P. (2003). Comparison of various precipitation downscaling methods for the
1021 simulation of streamflow in a rainshadow river basin. *International Journal of*
1022 *Climatology*, *23*(8), 887–901. https://doi.org/10.1002/joc.922

1023 Serreze, M. C., Clark, M. P., Armstrong, R. L., McGinnis, D. A., & Pulwarty, R. S. (1999).
1024 Characteristics of the western United States snowpack from snowpack telemetry
1025 (SNOTEL) data. *Water Resources Research*, *35*(7), 2145–2160.
1026 https://doi.org/10.1029/1999WR900090

1027 Stewart, I. T., Cayan, D. R., & Dettinger, M. D. (2005). Changes toward earlier streamflow
1028 timing across western North America. *Journal of Climate*, *18*(8), 1136–1155.
1029 https://doi.org/10.1175/JCLI3321.1

1030 Taylor, K. E., Stouffer, R. J., & Meehl, G. A. (2012). An overview of CMIP5 and the
1031 experiment design. *Bulletin of the American Meteorological Society*, *93*(4), 485–498.
1032 https://doi.org/10.1175/BAMS-D-11-00094.1

1033 Teutschbein, C., & Seibert, J. (2012). Bias correction of regional climate model simulations
1034 for hydrological climate-change impact studies: Review and evaluation of different
1035 methods. *Journal of Hydrology*, *456–457*, 12–29.
1036 https://doi.org/10.1016/j.jhydrol.2012.05.052

1037 Thrasher, B., Maurer, E. P., McKellar, C., & Duffy, P. B. (2012). Technical Note: Bias
1038 correcting climate model simulated daily temperature extremes with quantile mapping.
1039 *Hydrology and Earth System Sciences*, *16*(9), 3309–3314. https://doi.org/10.5194/hess-
1040 16-3309-2012

1041 Udall, B., & Overpeck, J. (2017). The twenty-first century Colorado River hot drought and
1042 implications for the future. *Water Resources Research*, *53*(3), 2404–2418.
1043 https://doi.org/10.1002/2016WR019638

1044 Wood, A. W., Maurer, E. P., Kumar, A., & Lettenmaier, D. P. (2002). Long-range
1045 experimental hydrologic forecasting for the eastern United States. *Journal of*
1046 *Geophysical Research: Atmospheres*, *107*(20), ACL 6-1-ACL 6-15.
1047 https://doi.org/10.1029/2001JD000659

1048 Yarnell, S. M., Petts, G. E., Schmidt, J. C., Whipple, A. A., Beller, E. E., Dahm, C. N., …
1049 Viers, J. H. (2015). Functional Flows in Modified Riverscapes: Hydrographs, Habitats
1050 and Opportunities. *BioScience*, *65*(10), 963–972. https://doi.org/10.1093/biosci/biv102

1051

1052